arXiv:1205.3018v3 [astro-ph.HE] 25 Jan 2013

A FIRST SEARCH FOR COINCIDENT GRAVITATIONAL WAVES AND HIGH ENERGY NEUTRINOS USING LIGO, Virgo AND ANTARES DATA FROM 2007

S. Adrián-Martínez[1], I. Al Samarai[2], A. Albert[3], M. André[4], M. Anghinolfi[5], G. Anton[6], S. Anvar[7], M. Ardid[1], T. Astraatmadja[8,39], J-J. Aubert[2], B. Baret[9], S. Basa[10], V. Bertin[2], S. Biagi[11,12], C. Bigongiari[13], C. Bogazzi[8], M. Bou-Cabo[1], B. Bouhou[9], M.C. Bouwhuis[8], J. Brunner[2], J. Busto[2], A. Capone[14,15], C. Cârloganu[16], J. Carr[2], S. Cecchini[11], Z. Charif[2], Ph. Charvis[17], T. Chiarusi[11], M. Circella[18], R. Coniglione[19], L. Core[2], H. Costantini[2], P. Coyle[2], A. Creusot[9], C. Curtil[2], G. De Bonis[14,15], M.P. Decowski[8], I. Dekeyser[20], A. Deschamps[17], C. Distefano[19], C. Donzaud[9,21], D. Dornic[13,2], Q. Dorosti[22], D. Drouhin[3], T. Eberl[6], U. Emanuele[13], A. Enzenhöfer[6], J-P. Ernenwein[2], S. Escoffier[2], K. Fehn[6], P. Fermani[14,15], M. Ferri[1], S. Ferry[23], V. Flaminio[24,25], F. Folger[6], U. Fritsch[6], J-L. Fuda[20], S. Galatà[2], P. Gay[16], K. Geyer[6], G. Giacomelli[11,12], V. Giordano[19], J.P. Gómez-González[13], K. Graf[6], G. Guillard[16], G. Hallewell[2], M. Hamal[26], H. van Haren[27], A.J. Heijboer[8], Y. Hello[17], J.J. Hernández-Rey[13], B. Herold[6], J. Hössl[6], C.C. Hsu[8], M. de Jong[8,39], M. Kadler[28], O. Kalekin[6], A. Kappes[6,40], U. Katz[6], O. Kavatsyuk[22], P. Kooijman[8,29,30], C. Kopper[8,6], A. Kouchner[9], I. Kreykenbohm[28], V. Kulikovskiy[31,5], R. Lahmann[6], G. Lambard[13], G. Larosa[1], D. Lattuada[19], D. Lefèvre[20], G. Lim[8,30], D. Lo Presti[32,33], H. Loehner[22], S. Loucatos[23], F. Louis[7], S. Mangano[13], M. Marcelin[10], A. Margiotta[11,12], J.A. Martínez-Mora[1], S. Martini[20], A. Meli[6], T. Montaruli[18,34], M. Morganti[24,41], L. Moscoso[9,23,†], H. Motz[6], M. Neff[6], E. Nezri[10], D. Palioselitis[8], G.E. Păvălaş[35], K. Payet[23], J. Petrovic[8], P. Piattelli[19], V. Popa[35], T. Pradier[36], E. Presani[8], C. Racca[3], C. Reed[8], G. Riccobene[19], C. Richardt[6], R. Richter[6], C. Rivière[2], A. Robert[20], K. Roensch[6], A. Rostovtsev[37], J. Ruiz-Rivas[13], M. Rujoiu[35], G.V. Russo[32,33], D.F.E. Samtleben[8], A. Sánchez-Losa[13], P. Sapienza[19], J. Schmid[6], J. Schnabel[6], F. Schöck[6], J-P. Schuller[23], F. Schüssler[23], T. Seitz[6], R. Shanidze[6], F. Simeone[14,15], A. Spies[6], M. Spurio[11,12], J.J.M. Steijger[8], Th. Stolarczyk[23], M. Taiuti[5,38], C. Tamburini[20], A. Trovato[32], B. Vallage[23], C. Vallée[2], V. Van Elewyck[9], M. Vecchi[2], P. Vernin[23], E. Visser[8], S. Wagner[6], G. Wijnker[8], J. Wilms[28], E. de Wolf[8,30], H. Yepes[13], D. Zaborov[37], J.D. Zornoza[13], J. Zúñiga[13]

The Antares Collaboration

J. Aasi[42], J. Abadie[42], B. P. Abbott[42], R. Abbott[42], T. D. Abbott[43], M. Abernathy[44], T. Accadia[45], F. Acernese[46,48], C. Adams[49], T. Adams[50], P. Addesso[48], R. Adhikari[42], C. Affeldt[52,53], M. Agathos[8], K. Agatsuma[55], P. Ajith[42], B. Allen[52,56,53], A. Allocca[24,57], E. Amador Ceron[56], D. Amariutei[58], S. B. Anderson[42], W. G. Anderson[56], K. Arai[42], M. C. Araya[42], S. Ast[52,53], S. M. Aston[49], P. Astone[14], D. Atkinson[59], P. Aufmuth[53,52], C. Aulbert[52,53], B. E. Aylott[60], S. Babak[61], P. Baker[62], G. Ballardin[63], S. Ballmer[64], Y. Bao[58], J. C. B. Barayoga[42], D. Barker[59], F. Barone[46,48], B. Barr[44], L. Barsotti[65], M. Barsuglia[9], M. A. Barton[59], I. Bartos[66], R. Bassiri[44,67], M. Bastarrika[44], A. Basti[24,25], J. Batch[59], J. Bauchrowitz[52,53], Th. S. Bauer[8], M. Bebronne[45], D. Beck[67], B. Behnke[61], M. Bejger[70], M.G. Beker[8], A. S. Bell[44], C. Bell[44], I. Belopolski[66], M. Benacquista[74], J. M. Berliner[59], A. Bertolini[52,53], J. Betzwieser[49], N. Beveridge[44], P. T. Beyersdorf[75], T. Bhadbade[67], I. A. Bilenko[76], G. Billingsley[42], J. Birch[49], R. Biswas[74], M. Bitossi[24], M. A. Bizouard[77], E. Black[42], J. K. Blackburn[42], L. Blackburn[79], D. Blair[80], B. Bland[59], M. Blom[8], O. Bock[52,53], T. P. Bodiya[65], C. Bogan[52,53], C. Bond[60], R. Bondarescu[81], F. Bondu[83], L. Bonelli[24,25], R. Bonnand[84], R. Bork[42], M. Born[52,53], V. Boschi[24], S. Bose[85], L. Bosi[86], S. Braccini[24,†], C. Bradaschia[24], P. R. Brady[56], V. B. Braginsky[76], M. Branchesi[88,89], J. E. Brau[90], J. Breyer[52,53], T. Briant[91], D. O. Bridges[49], A. Brillet[82], M. Brinkmann[52,53], V. Brisson[77], M. Britzger[52,53], A. F. Brooks[42], D. A. Brown[64], T. Bulik[69], H. J. Bulten[8,54], A. Buonanno[92], J. Burguet–Castell[93], D. Buskulic[45], C. Buy[9], R. L. Byer[67], L. Cadonati[94], G. Cagnoli[74,84], E. Calloni[46,47], J. B. Camp[79], P. Campsie[44], K. Cannon[95], B. Canuel[63], J. Cao[96], C. D. Capano[92], F. Carbognani[63], L. Carbone[60], S. Caride[97], S. Caudill[98], M. Cavaglià[99], F. Cavalier[77], R. Cavalieri[63], G. Cella[24], C. Cepeda[42], E. Cesarini[89], T. Chalermsongsak[42], P. Charlton[100], E. Chassande-Mottin[9], W. Chen[96], X. Chen[80], Y. Chen[101], A. Chincarini[5], A. Chiummo[63], H. S. Cho[102], J. Chow[104], N. Christensen[104], S. S. Y. Chua[103], C. T. Y. Chung[105], S. Chung[80], G. Ciani[58], F. Clara[59], D. E. Clark[67], J. A. Clark[94], J. H. Clayton[56], F. Cleva[82], E. Coccia[106,107], P.-F. Cohadon[91], C. N. Colacino[24,25], A. Colla[14,15], M. Colombini[15], A. Conte[14,15], R. Conte[48], D. Cook[59], T. R. Corbitt[65], M. Cordier[75], N. Cornish[62], A. Corsi[42], C. A. Costa[98,109], M. Coughlin[104], J.-P. Coulon[82], P. Couvares[64], D. M. Coward[80], M. Cowart[49], D. C. Coyne[42], J. D. E. Creighton[56], T. D. Creighton[74], A. M. Cruise[60], A. Cumming[44], L. Cunningham[44], E. Cuoco[63], R. M. Cutler[60], K. Dahl[52,53], M. Damjanic[52,53], S. L. Danilishin[80], S. D'Antonio[106], K. Danzmann[52,53], V. Dattilo[63], B. Daudert[42], H. Daveloza[74], M. Davier[77], E. J. Daw[110], R. Day[63], T. Dayanga[85], R. De Rosa[46,47], D. DeBra[67], G. Debreczeni[111], J. Degallaix[84], W. Del Pozzo[8], T. Dent[50], V. Dergachev[42], R. DeRosa[98], S. Dhurandhar[112], L. Di Fiore[46], A. Di Lieto[24,25], I. Di Palma[52,53], M. Di Paolo Emilio[106,108], A. Di Virgilio[24], M. Díaz[74], A. Dietz[45,99], F. Donovan[65], K. L. Dooley[52,53], S. Doravari[42], S. Dorsher[113], M. Drago[114,115], R. W. P. Drever[118], J. C. Driggers[42], Z. Du[96], J.-C. Dumas[80], S. Dwyer[65], T. Eberle[52,53], M. Edgar[44], M. Edwards[50], A. Effler[98], P. Ehrens[42], G. Endrőczi[111], R. Engel[42], T. Etzel[42], K. Evans[44], M. Evans[65], T. Evans[49], M. Factourovich[66], V. Fafone[106,107], S. Fairhurst[50], B. F. Farr[119], M. Favata[56], D. Fazi[119], H. Fehrmann[52,53], D. Feldbaum[58], I. Ferrante[24,25], F. Ferrini[63], F. Fidecaro[24,25], L. S. Finn[81], I. Fiori[63], R. P. Fisher[64], R. Flaminio[84], S. Foley[65], E. Forsi[49], L. A. Forte[46], N. Fotopoulos[42], J.-D. Fournier[82], J. Franc[84], S. Franco[77], S. Frasca[14,15], F. Frasconi[24], M. Frede[52,53], M. A. Frei[120], Z. Frei[121], A. Freise[60], R. Frey[90], T. T. Fricke[52,53], D. Friedrich[52,53], P. Fritschel[65], V. V. Frolov[49], M.-K. Fujimoto[55], P. J. Fulda[60], M. Fyffe[49], J. Gair[122], M. Galimberti[84], L. Gammaitoni[86,87],

J. Garcia[59], F. Garufi[46,47], M. E. Gáspár[111], G. Gelencser[121], G. Gemme[5], E. Genin[63], A. Gennai[24],
L. Á. Gergely[123], S. Ghosh[85], J. A. Giaime[98,49], S. Giampanis[56], K. D. Giardina[49], A. Giazotto[24], S. Gil-Casanova[93],
C. Gill[44], J. Gleason[58], E. Goetz[52,53], G. González[98], M. L. Gorodetsky[76], S. Gossler[52,53], R. Gouaty[45],
C. Graef[52,53], P. B. Graff[122], M. Granata[84], A. Grant[44], C. Gray[59], R. J. S. Greenhalgh[124], A. M. Gretarsson[125],
C. Griffo[43], H. Grote[52,53], K. Grover[60], S. Grunewald[61], G. M. Guidi[88,89], C. Guido[49], R. Gupta[112],
E. K. Gustafson[42], R. Gustafson[97], J. M. Hallam[60], D. Hammer[56], G. Hammond[44], J. Hanks[59], C. Hanna[42,126],
J. Hanson[49], J. Harms[118], G. M. Harry[127], I. W. Harry[64], E. D. Harstad[90], M. T. Hartman[58], K. Haughian[44],
K. Hayama[55], J.-F. Hayau[83], J. Heefner[42,†], A. Heidmann[91], M. C. Heintze[49], H. Heitmann[82], P. Hello[77],
G. Hemming[63], M. A. Hendry[44], I. S. Heng[44], A. W. Heptonstall[42], V. Herrera[67], M. Heurs[52,53], M. Hewitson[52,53],
S. Hild[44], D. Hoak[94], K. A. Hodge[42], K. Holt[49], M. Holtrop[128], T. Hong[101], S. Hooper[80], J. Hough[44],
E. J. Howell[80], B. Hughey[56], S. Husa[93], S. H. Huttner[44], T. Huynh-Dinh[49], D. R. Ingram[59], R. Inta[103], T. Isogai[104],
A. Ivanov[42], K. Izumi[55], M. Jacobson[42], E. James[42], Y. J. Jang[119], P. Jaranowski[71], E. Jesse[125], W. W. Johnson[98],
D. I. Jones[129], R. Jones[44], R.J.G. Jonker[8], L. Ju[80], P. Kalmus[42], V. Kalogera[119], S. Kandhasamy[113], G. Kang[130],
J. B. Kanner[92,79], M. Kasprzack[63,77], R. Kasturi[131], E. Katsavounidis[65], W. Katzman[49], H. Kaufer[52,53],
K. Kaufman[101], K. Kawabe[59], S. Kawamura[55], F. Kawazoe[52,53], D. Keitel[52,53], D. Kelley[64], W. Kells[42],
D. G. Keppel[42], Z. Keresztes[123], A. Khalaidovski[52,53], F. Y. Khalili[76], E. A. Khazanov[132], B. K. Kim[130], C. Kim[133],
H. Kim[52,53], K. Kim[134], N. Kim[67], Y. M. Kim[102], P. J. King[42], D. L. Kinzel[49], J. S. Kissel[65], S. Klimenko[58], J. Kline[56],
K. Kokeyama[98], V. Kondrashov[42], S. Koranda[56], W. Z. Korth[42], I. Kowalska[69], D. Kozak[42], V. Kringel[52,53],
B. Krishnan[61], A. Królak[68,72], G. Kuehn[52,53], P. Kumar[64], R. Kumar[44], R. Kurdyumov[67], P. Kwee[65], P. K. Lam[103],
M. Landry[59], A. Langley[118], B. Lantz[67], N. Lastzka[52,53], C. Lawrie[44], A. Lazzarini[42], A. Le Roux[49], P. Leaci[61],
C. H. Lee[102], H. K. Lee[134], H. M. Lee[135], J. R. Leong[52,53], I. Leonor[90], N. Leroy[77], N. Letendre[45], V. Lhuillier[59],
J. Li[96], T. G. F. Li[8], P. E. Lindquist[42], V. Litvine[42], Y. Liu[96], Z. Liu[58], N. A. Lockerbie[136], D. Lodhia[60], J. Logue[44],
M. Lorenzini[88], V. Loriette[78], M. Lormand[49], G. Losurdo[88], J. Lough[64], M. Lubinski[59], H. Lück[52,53],
A. P. Lundgren[52,53], J. Macarthur[44], E. Macdonald[44], B. Machenschalk[52,53], M. MacInnis[65], D. M. Macleod[50],
M. Mageswaran[42], K. Mailand[42], E. Majorana[14], I. Maksimovic[78], V. Malvezzi[106], N. Man[82], I. Mandel[60],
V. Mandic[113], M. Mantovani[24], F. Marchesoni[86], F. Marion[45], S. Márka[66], Z. Márka[66], A. Markosyan[67],
E. Maros[42], J. Marque[63], F. Martelli[88,89], I. W. Martin[44], R. M. Martin[58], J. N. Marx[42], K. Mason[65],
A. Masserot[45], F. Matichard[65], L. Matone[66], R. A. Matzner[137], N. Mavalvala[65], G. Mazzolo[52,53], R. McCarthy[59],
D. E. McClelland[103], S. C. McGuire[138], G. McIntyre[42], J. McIver[94], G. D. Meadors[97], M. Mehmet[52,53],
T. Meier[53,52], A. Melatos[105], A. C. Melissinos[139], G. Mendell[59], D. F. Menéndez[81], R. A. Mercer[56], S. Meshkov[42],
C. Messenger[50], M. S. Meyer[49], H. Miao[101], C. Michel[84], L. Milano[46,47], J. Miller[103], Y. Minenkov[106],
C. M. F. Mingarelli[60], V. P. Mitrofanov[76], G. Mitselmakher[58], R. Mittleman[65], B. Moe[56], M. Mohan[63],
S. R. P. Mohapatra[94], J. Moraru[59], G. Moreno[59], N. Morgado[84], A. Morgia[106,107], T. Mori[55], S. R. Morriss[74],
S. Mosca[46,47], K. Mossavi[52,53], B. Mours[45], C. M. Mow-Lowry[103], C. L. Mueller[58], G. Mueller[58], S. Mukherjee[74],
A. Mullavey[98,103], H. Müller-Ebhardt[52,53], J. Munch[140], D. Murphy[66], P. G. Murray[44], A. Mytidis[58], T. Nash[42],
L. Naticchioni[14,15], V. Necula[58], J. Nelson[44], I. Neri[86,87], G. Newton[44], T. Nguyen[103], A. Nishizawa[55], A. Nitz[64],
F. Nocera[63], D. Nolting[49], M. E. Normandin[74], L. Nuttall[50], E. Ochsner[56], J. O'Dell[124], E. Oelker[65],
G. H. Ogin[42], J. J. Oh[141], S. H. Oh[141], R. G. Oldenberg[56], B. O'Reilly[49], R. O'Shaughnessy[56], C. Osthelder[42],
C. D. Ott[101], D. J. Ottaway[140], R. S. Ottens[58], H. Overmier[49], B. J. Owen[81], A. Page[60], L. Palladino[106,108],
C. Palomba[14], Y. Pan[92], C. Pankow[56], F. Paoletti[24,63], R. Paoletti[24,57], M. A. Papa[61,56], M. Parisi[46,47],
A. Pasqualetti[63], R. Passaquieti[24,25], D. Passuello[24], M. Pedraza[42], S. Penn[131], A. Perreca[64], G. Persichetti[46,47],
M. Phelps[42], M. Pichot[82], M. Pickenpack[52,53], F. Piergiovanni[88,89], V. Pierro[51], M. Pihlaja[113], L. Pinard[84],
I. M. Pinto[51], M. Pitkin[44], H. J. Pletsch[52,53], M. V. Plissi[44], R. Poggiani[24,25], J. Pöld[52,53], F. Postiglione[48],
C. Poux[42], M. Prato[5], V. Predoi[50], T. Prestegard[113], L. R. Price[42], M. Prijatelj[52,53], M. Principe[51],
S. Privitera[42], R. Prix[52,53], G. A. Prodi[114,115], L. G. Prokhorov[76], O. Puncken[52,53], M. Punturo[86], P. Puppo[14],
V. Quetschke[74], R. Quitzow-James[90], F. J. Raab[59], D. S. Rabeling[8,54], I. Rácz[111], H. Radkins[59], P. Raffai[66,121],
M. Rakhmanov[74], C. Ramet[49], B. Rankins[99], P. Rapagnani[14,15], V. Raymond[119], V. Re[106,107], C. M. Reed[59],
T. Reed[142], T. Regimbau[82], S. Reid[44], D. H. Reitze[42], F. Ricci[14,15], R. Riesen[49], K. Riles[97], M. Roberts[67],
N. A. Robertson[42,44], F. Robinet[77], C. Robinson[50], E. L. Robinson[61], A. Rocchi[106], S. Roddy[49], C. Rodriguez[119],
M. Rodruck[59], L. Rolland[45], J. G. Rollins[42], J. D. Romano[74], R. Romano[46,48], J. H. Romie[49], D. Rosińska[70,73],
C. Röver[52,53], S. Rowan[44], A. Rüdiger[52,53], P. Ruggi[63], K. Ryan[59], F. Salemi[52,53], L. Sammut[105], V. Sandberg[59],
S. Sankar[65], V. Sannibale[42], L. Santamaría[42], I. Santiago-Prieto[44], G. Santostasi[143], E. Saracco[84], B. Sassolas[84],
B. S. Sathyaprakash[50], P. R. Saulson[64], R. L. Savage[59], R. Schilling[52,53], R. Schnabel[52,53], R. M. S. Schofield[90],
B. Schulz[52,53], B. F. Schutz[61,50], P. Schwinberg[59], J. Scott[44], S. M. Scott[103], F. Seifert[42], D. Sellers[49],
D. Sentenac[63], A. Sergeev[132], D. A. Shaddock[103], M. Shaltev[52,53], B. Shapiro[65], P. Shawhan[92], D. H. Shoemaker[65],
T. L Sidery[60], X. Siemens[56], D. Sigg[59], D. Simakov[52,53], A. Singer[42], L. Singer[42], A. M. Sintes[93], G. R. Skelton[56],
B. J. J. Slagmolen[103], J. Slutsky[98], J. R. Smith[43], M. R. Smith[42], R. J. E. Smith[60], N. D. Smith-Lefebvre[65],
K. Somiya[101], B. Sorazu[44], F. C. Speirits[44], L. Sperandio[106,107], M. Stefszky[103], E. Steinert[59], J. Steinlechner[52,53],
S. Steinlechner[52,53], S. Steplewski[85], A. Stochino[42], R. Stone[74], K. A. Strain[44], S. E. Strigin[76], A. S. Stroeer[74],
R. Sturani[88,89], A. L. Stuver[49], T. Z. Summerscales[144], M. Sung[98], S. Susmithan[80], P. J. Sutton[50], B. Swinkels[63],
G. Szeifert[121], M. Tacca[63], L. Taffarello[116], D. Talukder[85], D. B. Tanner[58], S. P. Tarabrin[52,53], R. Taylor[42],
A. P. M. ter Braack[8], P. Thomas[59], K. A. Thorne[49], K. S. Thorne[101], E. Thrane[113], A. Thüring[53,52], C. Titsler[81],
K. V. Tokmakov[136], C. Tomlinson[110], A. Toncelli[24,25], M. Tonelli[24,25], O. Torre[24,57], C. V. Torres[74],
C. I. Torrie[42,44], E. Tournefier[45], F. Travasso[86,87], G. Traylor[49], M. Tse[66], D. Ugolini[145], H. Vahlbruch[53,52],
G. Vajente[24,25], J. F. J. van den Brand[8,54], C. Van Den Broeck[8], S. van der Putten[8], A. A. van Veggel[44],
S. Vass[42], M. Vasuth[111], R. Vaulin[65], M. Vavoulidis[77], A. Vecchio[60], G. Vedovato[116], J. Veitch[50], P. J. Veitch[140],
K. Venkateswara[146], D. Verkindt[45], F. Vetrano[88,89], A. Viceré[88,89], A. E. Villar[42], J.-Y. Vinet[82], S. Vitale[8],
H. Vocca[86], C. Vorvick[59], S. P. Vyatchanin[76], A. Wade[103], L. Wade[56], M. Wade[56], S. J. Waldman[65], L. Wallace[42],
Y. Wan[96], M. Wang[60], X. Wang[96], A. Wanner[52,53], R. L. Ward[9], M. Was[77], M. Weinert[52,53], A. J. Weinstein[42],

R. Weiss[65], T. Welborn[49], L. Wen[101,80], P. Wessels[52,53], M. West[64], T. Westphal[52,53], K. Wette[52,53],
J. T. Whelan[120], S. E. Whitcomb[42,80], D. J. White[110], B. F. Whiting[58], K. Wiesner[52,53], C. Wilkinson[59],
P. A. Willems[42], L. Williams[58], R. Williams[42], B. Willke[52,53], M. Wimmer[52,53], L. Winkelmann[52,53],
W. Winkler[52,53], C. C. Wipf[65], A. G. Wiseman[56], H. Wittel[52,53], G. Woan[44], R. Wooley[49], J. Worden[59],
J. Yablon[119], I. Yakushin[49], H. Yamamoto[42], K. Yamamoto[115,117], C. C. Yancey[92], H. Yang[101], D. Yeaton-Massey[42],
S. Yoshida[147], M. Yvert[45], A. Zadrożny[72], M. Zanolin[125], J.-P. Zendri[116], F. Zhang[96], L. Zhang[42], C. Zhao[80],
N. Zotov[142,†], M. E. Zucker[65], J. Zweizig[42]

The LIGO Scientific Collaboration and the Virgo Collaboration

Draft version January 28, 2013

ABSTRACT

We present the results of the first search for gravitational wave bursts associated with high energy neutrinos. Together, these messengers could reveal new, hidden sources that are not observed by conventional photon astronomy, particularly at high energy. Our search uses neutrinos detected by the underwater neutrino telescope ANTARES in its 5 line configuration during the period January - September 2007, which coincided with the fifth and first science runs of LIGO and Virgo, respectively. The LIGO-Virgo data were analysed for candidate gravitational-wave signals coincident in time and direction with the neutrino events. No significant coincident events were observed. We place limits on the density of joint high energy neutrino - gravitational wave emission events in the local universe, and compare them with densities of merger and core-collapse events.

Subject headings: gravitational waves — high energy neutrinos

[1] Institut d'Investigació per a la Gestió Integrada de les Zones Costaneres (IGIC) - Universitat Politècnica de València. C/ Paranimf 1 , 46730 Gandia, Spain.

[2] CPPM, Aix-Marseille Université, CNRS/IN2P3, Marseille, France

[3] GRPHE - Institut universitaire de technologie de Colmar, 34 rue du Grillenbreit BP 50568 - 68008 Colmar, France

[4] Technical University of Catalonia, Laboratory of Applied Bioacoustics, Rambla Exposició, 08800 Vilanova i la Geltrú, Barcelona, Spain

[5] INFN - Sezione di Genova, Via Dodecaneso 33, 16146 Genova, Italy

[6] Friedrich-Alexander-Universität Erlangen-Nürnberg, Erlangen Centre for Astroparticle Physics, Erwin-Rommel-Str. 1, 91058 Erlangen, Germany

[7] Direction des Sciences de la Matière - Institut de recherche sur les lois fondamentales de l'Univers - Service d'Electronique des Détecteurs et d'Informatique, CEA Saclay, 91191 Gif-sur-Yvette Cedex, France

[8] Nikhef, Science Park, Amsterdam, The Netherlands

[9] APC, Université Paris Diderot, CNRS/IN2P3, CEA/IRFU, Observatoire de Paris, Sorbonne Paris Cité, 75205 Paris, France

[10] LAM - Laboratoire d'Astrophysique de Marseille, Pôle de l'Étoile Site de Château-Gombert, rue Frédéric Joliot-Curie 38, 13388 Marseille Cedex 13, France

[11] INFN - Sezione di Bologna, Viale C. Berti-Pichat 6/2, 40127 Bologna, Italy

[12] Dipartimento di Fisica dell'Università, Viale Berti Pichat 6/2, 40127 Bologna, Italy

[13] IFIC - Instituto de Física Corpuscular, Edificios Investigación de Paterna, CSIC - Universitat de València, Apdo. de Correos 22085, 46071 Valencia, Spain

[14] INFN -Sezione di Roma, P.le Aldo Moro 2, 00185 Roma, Italy

[15] Dipartimento di Fisica dell'Università La Sapienza, P.le Aldo Moro 2, 00185 Roma, Italy

[16] Clermont Université, Université Blaise Pascal, CNRS/IN2P3, Laboratoire de Physique Corpusculaire, BP 10448, 63000 Clermont-Ferrand, France

[17] Géoazur - Université de Nice Sophia-Antipolis, CNRS/INSU, IRD, Observatoire de la Côte d'Azur and Université Pierre et Marie Curie, BP 48, 06235 Villefranche-sur-mer, France

[18] INFN - Sezione di Bari, Via E. Orabona 4, 70126 Bari, Italy

[19] INFN - Laboratori Nazionali del Sud (LNS), Via S. Sofia 62, 95123 Catania, Italy

[20] MIO, Mediterranean Institute of Oceanography, Aix-Marseille University, 13288, Marseille, Cedex 9, France; Université du Sud Toulon-Var, 83957, La Garde Cedex, France

CNRS-INSU/IRD UM 110

[21] Univ Paris-Sud , 91405 Orsay Cedex, France

[22] Kernfysisch Versneller Instituut (KVI), University of Groningen, Zernikelaan 25, 9747 AA Groningen, The Netherlands

[23] Direction des Sciences de la Matière - Institut de recherche sur les lois fondamentales de l'Univers - Service de Physique des Particules, CEA Saclay, 91191 Gif-sur-Yvette Cedex, France

[24] INFN - Sezione di Pisa, Largo B. Pontecorvo 3, 56127 Pisa, Italy

[25] Dipartimento di Fisica dell'Università di Pisa, Largo B. Pontecorvo 3, 56127 Pisa, Italy

[26] University Mohammed I, Laboratory of Physics of Matter and Radiations, B.P.717, Oujda 6000, Morocco

[27] Royal Netherlands Institute for Sea Research (NIOZ), Landsdiep 4,1797 SZ 't Horntje (Texel), The Netherlands

[28] Dr. Remeis-Sternwarte and ECAP, Universität Erlangen-Nürnberg, Sternwartstr. 7, 96049 Bamberg, Germany

[29] Universiteit Utrecht, Faculteit Betawetenschappen, Princetonplein 5, 3584 CC Utrecht, The Netherlands

[30] Universiteit van Amsterdam, Instituut voor Hoge-Energie Fysica, Science Park 105, 1098 XG Amsterdam, The Netherlands

[31] Moscow State University, Skobeltsyn Institute of Nuclear Physics, Leninskie gory, 119991 Moscow, Russia

[32] INFN - Sezione di Catania, Viale Andrea Doria 6, 95125 Catania, Italy

[33] Dipartimento di Fisica ed Astronomia dell'Università, Viale Andrea Doria 6, 95125 Catania, Italy

[34] Département de Physique Nucléaire et Corpusculaire, Université de Genève, 1211, Geneva, Switzerland

[35] Institute for Space Sciences, R-77125 Bucharest, Măgurele, Romania

[36] IPHC-Institut Pluridisciplinaire Hubert Curien - Université de Strasbourg et CNRS/IN2P3 23 rue du Loess, BP 28, 67037 Strasbourg Cedex 2, France

[37] ITEP - Institute for Theoretical and Experimental Physics, B. Cheremushkinskaya 25, 117218 Moscow, Russia

[38] Dipartimento di Fisica dell'Università, Via Dodecaneso 33, 16146 Genova, Italy

[39] Also at University of Leiden, the Netherlands

[40] On leave of absence at the Humboldt-Universität zu Berlin

[41] Also at Accademia Navale di Livorno, Livorno, Italy

[42] LIGO - California Institute of Technology, Pasadena, CA 91125, USA

[43] California State University Fullerton, Fullerton CA 92831 USA

[44] SUPA, University of Glasgow, Glasgow, G12 8QQ, United Kingdom

[45] Laboratoire d'Annecy-le-Vieux de Physique des Particules

(LAPP), Université de Savoie, CNRS/IN2P3, F-74941 Annecy-Le-Vieux, France

[46] INFN, Sezione di Napoli, Complesso Universitario di Monte S.Angelo, I-80126 Napoli, Italy

[47] Università di Napoli 'Federico II', Complesso Universitario di Monte S.Angelo, I-80126 Napoli, Italy

[48] Università di Salerno, I-84084 Fisciano (Salerno), Italy

[49] LIGO - Livingston Observatory, Livingston, LA 70754, USA

[50] Cardiff University, Cardiff, CF24 3AA, United Kingdom

[51] University of Sannio at Benevento, I-82100 Benevento, Italy and INFN (Sezione di Napoli), Italy

[52] Albert-Einstein-Institut, Max-Planck-Institut für Gravitationsphysik, D-30167 Hannover, Germany

[53] Leibniz Universität Hannover, D-30167 Hannover, Germany

[54] VU University Amsterdam, De Boelelaan 1081, 1081 HV Amsterdam, the Netherlands

[55] National Astronomical Observatory of Japan, Tokyo 181-8588, Japan

[56] University of Wisconsin–Milwaukee, Milwaukee, WI 53201, USA

[57] Università di Siena, I-53100 Siena, Italy

[58] University of Florida, Gainesville, FL 32611, USA

[59] LIGO - Hanford Observatory, Richland, WA 99352, USA

[60] University of Birmingham, Birmingham, B15 2TT, United Kingdom

[61] Albert-Einstein-Institut, Max-Planck-Institut für Gravitationsphysik, D-14476 Golm, Germany

[62] Montana State University, Bozeman, MT 59717, USA

[63] European Gravitational Observatory (EGO), I-56021 Cascina (PI), Italy

[64] Syracuse University, Syracuse, NY 13244, USA

[65] LIGO - Massachusetts Institute of Technology, Cambridge, MA 02139, USA

[66] Columbia University, New York, NY 10027, USA

[67] Stanford University, Stanford, CA 94305, USA

[68] IM-PAN 00-956 Warsaw, Poland

[69] Astronomical Observatory Warsaw University 00-478 Warsaw, Poland

[70] CAMK-PAN 00-716 Warsaw, Poland

[71] Białystok University 15-424 Białystok, Poland

[72] NCBJ 05-400 Świerk-Otwock, Poland

[73] Institute of Astronomy 65-265 Zielona Góra, Poland

[74] The University of Texas at Brownsville, Brownsville, TX 78520, USA

[75] San Jose State University, San Jose, CA 95192, USA

[76] Moscow State University, Moscow, 119992, Russia

[77] LAL, Université Paris-Sud, IN2P3/CNRS, F-91898 Orsay, France

[78] ESPCI, CNRS, F-75005 Paris, France

[79] NASA/Goddard Space Flight Center, Greenbelt, MD 20771, USA

[80] University of Western Australia, Crawley, WA 6009, Australia

[81] The Pennsylvania State University, University Park, PA 16802, USA

[82] Université Nice-Sophia-Antipolis, CNRS, Observatoire de la Côte d'Azur, F-06304 Nice, France

[83] Institut de Physique de Rennes, CNRS, Université de Rennes 1, 35042 Rennes, France

[84] Laboratoire des Matériaux Avancés (LMA), IN2P3/CNRS, F-69622 Villeurbanne, Lyon, France

[85] Washington State University, Pullman, WA 99164, USA

[86] INFN, Sezione di Perugia, I-06123 Perugia, Italy

[87] Università di Perugia, I-06123 Perugia, Italy

[88] INFN, Sezione di Firenze, I-50019 Sesto Fiorentino, Italy

[89] Università degli Studi di Urbino 'Carlo Bo', I-61029 Urbino, Italy

[90] University of Oregon, Eugene, OR 97403, USA

[91] Laboratoire Kastler Brossel, ENS, CNRS, UPMC, Université Pierre et Marie Curie, 4 Place Jussieu, F-75005 Paris, France

[92] University of Maryland, College Park, MD 20742 USA

[93] Universitat de les Illes Balears, E-07122 Palma de Mallorca, Spain

[94] University of Massachusetts - Amherst, Amherst, MA 01003, USA

[95] Canadian Institute for Theoretical Astrophysics, University of Toronto, Toronto, Ontario, M5S 3H8, Canada

[96] Tsinghua University, Beijing 100084 China

[97] University of Michigan, Ann Arbor, MI 48109, USA

[98] Louisiana State University, Baton Rouge, LA 70803, USA

[99] The University of Mississippi, University, MS 38677, USA

[100] Charles Sturt University, Wagga Wagga, NSW 2678, Australia

[101] Caltech-CaRT, Pasadena, CA 91125, USA

[102] Pusan National University, Busan 609-735, Korea

[103] Australian National University, Canberra, ACT 0200, Australia

[104] Carleton College, Northfield, MN 55057, USA

[105] The University of Melbourne, Parkville, VIC 3010, Australia

[106] INFN, Sezione di Roma Tor Vergata, I-00133 Roma, Italy

[107] Università di Roma Tor Vergata, I-00133 Roma, Italy

[108] Università dell'Aquila, I-67100 L'Aquila, Italy

[109] Instituto Nacional de Pesquisas Espaciais, 12227-010 - São José dos Campos, SP, Brazil

[110] The University of Sheffield, Sheffield S10 2TN, United Kingdom

[111] Wigner RCP, RMKI, H-1121 Budapest, Konkoly Thege Miklós út 29-33, Hungary

[112] Inter-University Centre for Astronomy and Astrophysics, Pune - 411007, India

[113] University of Minnesota, Minneapolis, MN 55455, USA

[114] INFN, Gruppo Collegato di Trento, I-38050 Povo, Trento, Italy

[115] Università di Trento, I-38050 Povo, Trento, Italy

[116] INFN, Sezione di Padova, I-35131 Padova, Italy

[117] Università di Padova, I-35131 Padova, Italy

[118] California Institute of Technology, Pasadena, CA 91125, USA

[119] Northwestern University, Evanston, IL 60208, USA

[120] Rochester Institute of Technology, Rochester, NY 14623, USA

[121] Eötvös Loránd University, Budapest, 1117 Hungary

[122] University of Cambridge, Cambridge, CB2 1TN, United Kingdom

[123] University of Szeged, 6720 Szeged, Dóm tér 9, Hungary

[124] Rutherford Appleton Laboratory, HSIC, Chilton, Didcot, Oxon OX11 0QX United Kingdom

[125] Embry-Riddle Aeronautical University, Prescott, AZ 86301 USA

[126] Perimeter Institute for Theoretical Physics, Ontario, N2L 2Y5, Canada

[127] American University, Washington, DC 20016, USA

[128] University of New Hampshire, Durham, NH 03824, USA

[129] University of Southampton, Southampton, SO17 1BJ, United Kingdom

[130] Korea Institute of Science and Technology Information, Daejeon 305-806, Korea

[131] Hobart and William Smith Colleges, Geneva, NY 14456, USA

[132] Institute of Applied Physics, Nizhny Novgorod, 603950, Russia

[133] Lund Observatory, Box 43, SE-221 00, Lund, Sweden

1. INTRODUCTION

Multi-messenger astronomy is entering a stimulating period with the recent development of experimental techniques that will open new windows of cosmic radiation observation in all its components. In particular, both high-energy ($\gg$ GeV) neutrinos (HENs) and gravitational waves (GWs), neither of which have yet been directly observed from astrophysical sources, are becoming new tools for exploring the Universe.

While HENs are expected to be produced in interactions between relativistic protons and the external radiation field of the source (e.g., Waxman & Bahcall 1997; Hümmer et al. 2012), GWs carry information on the intricate multi-dimensional dynamics in the source's central regions (e.g., Creighton & Anderson 2011). HENs and GWs are thus complementary messengers.

Simultaneous emission of GWs and HENs has been proposed in a range of cataclysmic cosmic events including gamma-ray bursts (GRBs), core-collapse supernovae (CCSNe), soft-gamma repeater outbursts (SGRs), and, potentially, cosmic string cusps in the early universe.

Observational constraints on HEN and GW emission from some of these phenomena have already been obtained. The IceCube collaboration recently placed limits on the HEN emission in GRBs (Abbasi et al. 2012a, 2011b, 2010), SGRs and blazars (Abbasi et al. 2012c), and jet-driven CCSNe (Abbasi et al. 2012b) using data from the IceCube detector at various levels of completion. Similarly, the ANTARES Collaboration has placed limits on the HEN flux from gamma-ray flaring blazars (Adrián-Martínez et al. 2012a) and GRBs (Adrián-Martínez et al. 2011), as well as a diffuse muon neutrino flux from extragalactic sources (Aguilar et al. 2011a). These limits, however, do not yet strongly constrain HEN emission and ultra-high-energy cosmic-ray production in relativistic outflows (Hümmer et al. 2012; Li 2012; He et al. 2012). The LIGO Scientific Collaboration and Virgo placed limits on the GW emission in GRBs (Abbott et al. 2010; Abadie et al. 2010a, 2012b) and SGRs (Abadie et al. 2011; Abbott et al. 2009c, 2008b). The exclusion distances of these searches were, however, not sufficiently large to expect a GW detection.

The above HEN and GW searches used timing and sky location information from observations of events in the electromagnetic spectrum. A potentially large subset of GW and HEN sources may be intrinsically electromag-netically faint, dust-obscured, or missed by telescopes, but sufficiently luminous in GWs and HEN to be detected. Such sources may include, but are not limited to, partially or completely choked GRBs with, perhaps, only mildly relativistic jets (Ando & Beacom 2005; Razzaque et al. 2005b; Murase et al. 2006; Wang et al. 2007), relativistic shock breakout in compact CCSN progenitor stars (Waxman & Loeb 2001), and cosmic string cusps (Damour & Vilenkin 2000; Siemens et al. 2006; Berezinsky et al. 2011).

Searches for HENs and GWs from such events have thus far relied on blind (i.e., untriggered) all-sky searches. Abbasi et al. (2012c) performed an all-sky search for point sources of HENs in IceCube data and Adrián-Martínez et al. (2012b) carried out a similar study with ANTARES data. LIGO and Virgo have carried out a number of all-sky searches for GWs. The most recent and most sensitive such search for model-independent GW bursts was published in Abadie et al. (2012a), whereas the most recent all-sky search for binary inspiral-merger is Abadie et al. (2012c). All-sky model-dependent constraints on cosmic string GW emission have been placed by Abbott et al. (2009a). The sensitivity of such blind all-sky searches is limited by a much larger background compared to searches based on timing and sky locations from electromagnetic observations.

A search for *temporally and spatially coincident* HEN and GW signals is a strong alternative to electromagnetically triggered or blind all-sky analyses that search for GWs or HENs individually. Such a search is independent of bias from electromagnetic observations, but still enjoys a much reduced background thanks to timing and sky location constraints. A similar idea has been used in the follow-up of candidate GW events by the low-energy neutrino detector LVD (Aglietta et al. 2004). A joint GW-HEN search was first proposed by Aso et al. (2008) and Pradier (2009), and Bartos et al. (2011) have derived constraints on joint GW-HEN signals based on the interpretation of independent GW and HEN observational results. Here we present the first direct search for coincident GW-HEN events, using data taken by the ANTARES HEN telescope and by the LIGO and Virgo GW observatories from January to September 2007. At this time, ANTARES was still under construction and operating with only 5 active lines. At the same time, the fifth LIGO science run (S5) and the first Virgo science run (VSR1) were carried out. This was the first joint run of the LIGO-Virgo network with the detectors operating near their design sensitivities.

The basic principle of the analysis presented here is that of a "triggered" search: HEN candidates are identified in the ANTARES data, then the GW data around the time of the HEN event are analyzed for a GW incident from the HEN estimated arrival direction. This method has been applied previously in searches for GWs associated with GRB triggers (Abbott et al. 2010; Abadie et al. 2012b). It has been shown to have a distance reach up to a factor of 2 larger (Abadie et al. 2012b) than a blind all-sky search of the GW data, due to the reduced background. The expected rate of detections depends also on the beaming of the trigger signal, since the triggered search is only sensitive to the subset of sources oriented towards Earth. Was (2011) compares the analysis method used in this paper to the LIGO-Virgo blind

[134] Hanyang University, Seoul 133-791, Korea

[135] Seoul National University, Seoul 151-742, Korea

[136] University of Strathclyde, Glasgow, G1 1XQ, United Kingdom

[137] The University of Texas at Austin, Austin, TX 78712, USA

[138] Southern University and A&M College, Baton Rouge, LA 70813, USA

[139] University of Rochester, Rochester, NY 14627, USA

[140] University of Adelaide, Adelaide, SA 5005, Australia

[141] National Institute for Mathematical Sciences, Daejeon 305-390, Korea

[142] Louisiana Tech University, Ruston, LA 71272, USA

[143] McNeese State University, Lake Charles, LA 70609 USA

[144] Andrews University, Berrien Springs, MI 49104 USA

[145] Trinity University, San Antonio, TX 78212, USA

[146] University of Washington, Seattle, WA, 98195-4290, USA

[147] Southeastern Louisiana University, Hammond, LA 70402, USA

[†] Deceased

all-sky search (Abadie et al. 2012a) and predicts a detection rate for the triggered search of between ∼0.1 and ∼6 times that of the blind search for beaming angles in the range $5° - 30°$. These numbers are broadly consistent with estimates for the special case of dedicated matched-filter searches for compact binary coalescence signals associated with short GRBs (eg Chen & Holz 2012; Kelley et al. 2012; Dietz et al. 2012; Nissanke et al. 2012) after rescaling for a smaller distance improvement factor (typically ∼1.3, due to the better inherent background rejection of these specialised searches). In either case, most of the GW events found by the triggered search will be new detections not found by the all-sky blind search, illustrating the value of the triggered search even when the relative detection rate is low (Was 2011).

We analyze a total of 158 HEN events detected at times when two or more of the LIGO-Virgo detectors were operating. ANTARES is sensitive to HENs with energies greater than ∼ 100 GeV (Adrián-Martínez et al. 2012c). The LIGO-Virgo analysis targets model-independent burst GW signals with durations ≲ 1 s and frequencies in the 60 Hz to 500 Hz band. The GW search is extended in frequency up to 2000 Hz only for a subset of the HEN events, because the computational cost of such a search with the current GW analysis pipeline is prohibitive.

Statistical analyses of the HEN sample show no sign of associated GW bursts.

This paper is organized as follows. In Section 2 we discuss sources of coincident HEN and GW emission and expected prospects for their detection. In Section 3 we describe the ANTARES, LIGO, and Virgo detectors and the joint data taking period. Section 4 describes how the HEN sample was selected. Section 5 describes the search for GWs coincident in time and direction with the HEN events. We present the results of the search in Section 6. We discuss the astrophysical implications of the results in Section 7 and conclude with considerations of the potential for future joint GW-HEN searches.

2. CANDIDATE SOURCES FOR HIGH-ENERGY NEUTRINO AND GRAVITATIONAL WAVE EMISSION

HEN emission is expected from baryon-loaded relativistic astrophysical outflows. In the most common scenario (e.g., Waxman & Bahcall 1997), Fermi-accelerated relativistic protons interact with high-energy outflow photons in $p\gamma$ reactions leading to pions or kaons, whose decay results in neutrinos, e.g., $\pi^+ \rightarrow \mu^+ + \nu_\mu \rightarrow e^+ + \nu_e + \bar{\nu}_\mu + \nu_\mu$, which is the dominant process (see, e.g., Winter 2012). This gives $(\nu_e + \bar{\nu}_e : \nu_\mu + \bar{\nu}_\mu : \nu_\tau + \bar{\nu}_\tau)$ production ratios of $(1 : 2 : 0)$, changing to approximately $(1 : 1 : 1)$ at Earth due to flavor oscillations (e.g., Athar et al. 2006). The HEN spectrum depends on the spectrum of the accelerated protons (e.g., Guetta et al. 2004; Abbasi et al. 2010; Hümmer et al. 2012) and, thus, on the properties of the astrophysical source. In this section, we provide estimates of the sensitivity of the 5-line ANTARES detector for HENs from the various potential sources by estimating the probability $P = X\%$ that at least one HEN is detected for a source at a given distance d_X.

GW emission occurs, at lowest and generally dominant order, via accelerated quadrupolar mass-energy dynamics. The coupling constant in the standard quadrupole formula for GW emission (e.g., Thorne 1987) is $Gc^{-4} \approx 10^{-49} \, \text{s}^2 \, \text{g}^{-1} \, \text{cm}^{-1}$ and the directly detectable GW strain scales with $(\text{distance})^{-1}$. For example, a source at 10 Mpc needs a quadrupole moment of $\sim 1 M_\odot \times (100 \, \text{km})^2$ that is changing on a millisecond timescale to be detectable by a GW detector sensitive to a strain of 10^{-21}. Equivalently, the minimum GW energy emission detectable by the LIGO-Virgo network at this distance is approximately $E_{\text{GW}} \simeq 10^{-2} M_\odot c^2$ to $10 M_\odot c^2$ for frequencies between 100 Hz and 1000 Hz (Abadie et al. 2012a).

In the following, we discuss a number of astrophysical scenarios in which both HENs and GWs may be emitted at detectable levels.

2.1. Canonical Long Gamma-Ray Bursts from Massive Stars

Long-duration GRBs (LGRBs; $T_{90} \gtrsim 2 \, \text{s}$; T_{90} is the time over which 90% of the γ counts are detected) are observationally implicated to be related to the collapse of massive stars normally leading to core-collapse supernova explosions (Hjorth & Bloom 2011; Modjaz 2011). Typical LGRBs are strongly beamed and most likely have jets with Lorentz factors $\Gamma \gtrsim 100$ and isotropic equivalent luminosities of $10^{51} \, \text{erg s}^{-1}$ to $10^{53} \, \text{erg s}^{-1}$ (Piran 2005; Mészáros 2006; Gehrels et al. 2009). LGRBs are detected at a rate of order 1/(few days) by γ-ray monitors on satellite observatories such as Swift/BAT (Gehrels et al. 2004; Barthelmy et al. 2005) and Fermi/GBM (Meegan et al. 2009; Bhat et al. 2004). It is important to note, however, that Swift/BAT and Fermi/GBM miss ∼90% and ∼40% of the prompt emission of all GRBs, respectively. This is due to limited fields of view, technical downtime, and orbital passes through the South Atlantic Anomaly. A nearby (say ∼10 Mpc) LGRB will have a bright multi-wavelength afterglow and may be accompanied by a CCSN (see §2.2), but a significant fraction of local CCSNe may have been missed by CCSN surveys based on galaxy catalogs (Mattila et al. 2012).

The central engine of LGRBs is expected to either be a *collapsar* (a black hole with an accretion disk; Woosley 1993; MacFadyen & Woosley 1999) or a *millisecond magnetar* (an extremely rapidly spinning, extremely magnetized neutron star; e.g., Metzger et al. 2011). In both scenarios, HEN emission may result from a relativistic expanding fireball. HENs may begin to be produced even before the jet breaks out of the stellar envelope (Razzaque et al. 2003) and may continue well into the afterglow phase (Murase & Nagataki 2006).

HEN emission from canonical LGRBs is expected to have appreciable flux for energies in the range 100 GeV to 100 TeV. For a LGRB at ∼50 Mpc (∼10 Mpc) one would expect of order 1 (100) HEN events in a km³-scale water- or ice-Cherenkov detector (e.g., Waxman & Bahcall 1997; Guetta et al. 2004; Hümmer et al. 2012; Abbasi et al. 2010). Based on the flux predictions of Guetta et al. (2004), the probability for detection in the 5-line ANTARES detector can be estimated to be ∼50% for a source at 10 Mpc, which decreases to ∼2% for a source at 50 Mpc. Note that these are most likely optimistic estimates, since more detailed analyses suggest lower HEN fluxes from GRBs (e.g., Hümmer et al. 2012).

The most extreme scenario for GW emission in LGRBs

is dynamical fragmentation of a collapsing extremely rapidly differentially spinning stellar core into a coalescing system of two protoneutron stars (Davies et al. 2002; Kobayashi & Mészáros 2003). Such a scenario may be unlikely given model predictions for the rotational configuration of GRB progenitor stars (e.g., Woosley & Heger 2006). Its GW emission, however, would be very strong, leading to emitted energies $E_{\rm GW} \sim 10^{-2} \, M_\odot c^2$ to $10^{-1} \, M_\odot c^2$ in the 50 Hz to 1000 Hz frequency band of highest sensitivity of the initial LIGO/Virgo detectors, which could observe such an event out to approximately 20 Mpc to 40 Mpc (Abadie et al. 2012c,b).

In more moderate scenarios backed by computational models, GW emission from LGRBs is likely to proceed, at least initially, in a very similar fashion as in a rapidly spinning CCSN (Ott 2009; Fryer & New 2011; Kotake 2011). If a black hole with an accretion disk forms, a second phase of GW emission may come from various hydrodynamic instabilities in the accretion disk (e.g., van Putten et al. 2004; Piro & Pfahl 2007; Kiuchi et al. 2011).

In the initial collapse of the progenitor star's core, a rapidly rotating protoneutron star is formed. In this process, a linearly-polarized GW signal is emitted with typical GW strains $|h| \sim 10^{-21}$ to 10^{-20} at a source distance of 10 kpc and emitted energies $E_{\rm GW} \sim 10^{-8} \, M_\odot c^2$ to $10^{-7} \, M_\odot c^2$ between 100 Hz and 1000 Hz (Dimmelmeier et al. 2008; Ott et al. 2012). This part of the GW signal will only be detectable for Galactic events and is thus not relevant here.

In its early evolution, the protoneutron star (or protomagnetar, depending on its magnetic field) may be spinning near breakup. This can induce various rotational instabilities that induce ellipsoidal deformations of the protoneutron star, leading to strong, quasi-periodic, elliptically-polarized GW emission (Fryer et al. 2002; Corsi & Mészáros 2009; Ott 2009; Scheidegger et al. 2010; Fryer & New 2011). A typical GW strain for a deformed protoneutron star of $1.4 \, M_\odot$ and radius of 12 km, spinning with a period of 1 ms may be $h \sim$ few $\times 10^{-22}$ at 10 Mpc. If the deformation lasted for 100 ms, $E_{\rm GW} \sim 10^{-1} \, M_\odot c^2$ would be emitted at 2000 Hz (Fryer et al. 2002).

In the collapsar scenario, accretion onto the protoneutron star eventually leads to its collapse to a spinning black hole (O'Connor & Ott 2011). This and the subsequent ringdown of the newborn black hole leads to a GW burst at few $\times 10^2$ Hz to few $\times 10^3$ Hz with $h \sim 10^{-20}$ at 10 kpc and $E_{\rm GW} \sim 10^{-7} \, M_\odot c^2$. It is thus detectable only for a Galactic source (Ott et al. 2011).

More interesting are hydrodynamic instabilities in the accretion disk/torus that forms after seconds of hyperaccretion onto the newborn black hole. The inner parts of the disk are hot, efficiently neutrino cooled and thus thin (e.g., Popham et al. 1999) while the outer regions are inefficiently cooled and form a thick accretion torus. Gravitational instability may lead to fragmentation of this torus into one or multiple overdense regions that may could condense to neutron-star-like objects and then inspiral into the central black hole (Piro & Pfahl 2007). For a source at 10 Mpc, a $1 M_\odot$ fragment and a $8 M_\odot$ central black hole, this would yield strains of $h \sim$ few $\times 10^{-22}$ and emitted energies in the most sensitive band of $\sim 10^{-3} \, M_\odot c^2$ to $10^{-2} \, M_\odot c^2$.

The accretion torus may be unstable to the Papaloizou-Pringle instability or to co-rotation-type instabilities (Papaloizou & Pringle 1984; Papaloizou & Savonije 1991). Kiuchi et al. (2011) estimated $h \sim 10^{-21}$ to 10^{-20} for a source at 10 Mpc and GW frequencies of 100 Hz to 200 Hz for a $m = 1$–dominated non-axisymmetric disk instability in a disk around a $10 \, M_\odot$ black hole. This corresponds to $E_{\rm GW}$ of order $10^{-2} \, M_\odot c^2$ to $10^{-1} \, M_\odot c^2$.

In the speculative suspended accretion model for GRB accretion disks (van Putten et al. 2004), low-order turbulence powered by black-hole spindown may emit strong GWs. In the frequency domain, this results in an anti-chirp behavior, since most of the emission is expected to occur near the innermost stable orbit, which moves out in radius as the black hole is spun down. Simple estimates suggest GW strains $h \sim 10^{-21}$ at 10 Mpc and frequencies in the 100 Hz to 1000 Hz band. Depending on the initial black hole spin, $E_{\rm GW}$ could be of order $1 \, M_\odot c^2$.

2.2. Low-Luminosity GRBs and Engine-Driven Supernovae

Low-luminosity GRBs (LL-GRBs; also frequently referred to as X-ray flashes) form a subclass of long GRBs with low γ-ray flux (e.g., Coward 2005; Hjorth & Bloom 2011; Modjaz 2011). LL-GRBs are much more easily missed by observations than LGRBs (see §2.1) and the small observable volume (due to their low luminosity) suggests an event rate that may be significantly higher than the rate of canonical LGRBs (Soderberg et al. 2006; Chapman et al. 2007; Le & Dermer 2007; Liang et al. 2007; Virgili et al. 2009). Five of the seven GRBs that have been unambiguously associated with a CCSN are LL-GRBs (Hjorth & Bloom 2011; Modjaz 2011; Zhang et al. 2012). Moreover, all GRB-CCSNe are highly energetic and of the spectroscopic type Ic-bl subclass. Ic indicates a compact hydrogen/helium poor progenitor star and the postfix -bl stands for "broad line," because they have relativistically Doppler-broadened spectral features.

Type Ic-bl CCSNe occur also without LL-GRB or LGRB, but are frequently identified as *engine-driven CCSNe* that exhibit luminous radio emission (e.g., Soderberg et al. 2006; Soderberg et al. 2010).

Theory suggests (e.g., Khokhlov et al. 1999; Burrows et al. 2007; Lazzati et al. 2012; Bromberg et al. 2011) that the transition between engine-driven CCSNe, LL-GRBs with CCSNe, and canonical LGRBs may be continuous. All are likely to be driven by a central engine that launches a collimated bipolar jet-like outflow and their variety may simply depend on the power output and duration of central engine operation (Lazzati et al. 2012; Bromberg et al. 2011). The power output of the engine determines the energy of the jet and its Lorentz factor. The duration of the central engine's operation determines if the jet can leave the progenitor star and make a normal LGRB. If it fails to emerge, the LGRB is "choked" and a more isotropic energetic CCSN explosion is likely to result. As suggested by Bromberg et al. (2011), the relativistic shock breakout through the stellar surface could then be responsible for a LL-GRB.

The GW emission processes that may be active in LL-GRBs and engine-driven CCSNe are most likley very similar to the LGRB case discussed in §2.1 and we shall not consider them further here. HEN emission is expected from the entire range of stellar collapse out-

comes involving relativistic flows. Since LL-GRBs and engine-driven CCSNe are most likely much more frequent that canonical LGRBs, much effort has been devoted to understanding the HEN emission from such events (Meszaros & Waxman 2001; Waxman & Loeb 2001; Razzaque et al. 2003; Ando & Beacom 2005; Razzaque et al. 2005a,b; Murase et al. 2006; Murase & Nagataki 2006; Wang et al. 2007; Horiuchi & Ando 2008). It is worthwhile to consider the probability of detection of HENs in the 5-line ANTARES detector from LL-GRBs and engine-driven CCSNe, in which mildly relativistic jets are likely to be involved. The detection probability depends strongly on the energy and the Lorentz factor of the jet. Using the reference parameters of Ando & Beacom (2005), $\Gamma = 3$ and $E_{\mathrm{jet}} = E_0 \approx 3 \times 10^{51}$ erg, the detection probability is $\sim 50\%$ at $d_{50} = 1\,\mathrm{Mpc}$.

2.3. Mergers and Short Gamma-Ray Bursts

Short-duration GRBs (SGRBs; $T_{90} \lesssim 2\,\mathrm{s}$) are rarer than LGRBs and expected to result from double neutron star (NS-NS) and/or neutron star – black hole (BH-NS) mergers (e.g., Nakar 2007; Gehrels et al. 2009). The isotropic equivalent energy of SGRBs is 2 to 3 orders of magnitude smaller than the energy of LGRBs. Their jets have most likely lower Lorentz factors of $\Gamma \sim 10$ to 50 and wider opening angles. Due to their short duration and low isotropic equivalent energy, SGRBs are much easier to miss observationally than LGRBs and their observable volume is much smaller.

The efficiency of HEN emission in SGRBs depends on the efficiency of proton acceleration, the γ-ray flux, and the SGRB variability time scale (Nakar 2007). For a simple estimate of the detection probability in the 5-line ANTARES detector, one may resort to the HEN flux estimates of Guetta et al. (2004) (but see Hümmer et al. 2012 for refined results). Assuming a jet with $\Gamma = 300$, $E_{\mathrm{jet}} = 2 \times 10^{50}$ erg, one finds a distance $d_{10} \sim 10\,\mathrm{Mpc}$ at which the probability of HEN detection by the 5-line ANTARES detector is 10%. Hence, only the closest and/or the most powerful SGRBs may be detectable.

The GW emission from NS-NS and BH-NS mergers is well studied (see Shibata & Taniguchi 2011; Faber & Rasio 2012, for reviews). Most of the emission comes from the late inspiral and merger phase during which the binary sweeps through the $50\,\mathrm{Hz}$ to $1000\,\mathrm{Hz}$ band of highest sensitivity of LIGO/Virgo. The total emitted E_{GW} is of order $10^{-2}\,M_\odot c^2$ to $10^{-1}\,M_\odot c^2$. At the time of this analysis the LIGO/Virgo network had maximum sensitive distances of $\sim 30\,\mathrm{Mpc}$ for equal-mass NS-NS binaries and $\sim 50\,\mathrm{Mpc}$ for a BH-NS binary with a mass ratio of $4:1$, and a dedicated merger search on this data did not find any evidence for GW candidates (Abadie et al. 2010b).

2.4. Bursting Magnetars

Soft-gamma repeaters (SGRs) and anomalous X-ray pulsars are X-ray pulsars with quiescent soft $(2-10\,\mathrm{keV})$ periodic X-ray emissions with periods ranging from 5 to $10\,\mathrm{s}$. They exhibit repetitive outbursts lasting $\sim 0.1\,\mathrm{s}$ which reach peak luminosities of $\sim 10^{42}\,\mathrm{erg\,s^{-1}}$ in X-rays and γ-rays. There are a number of known SGRs and anomalous X-ray pulsars (Hurley 2011; Mereghetti 2011), some of which have had rare hard spectrum gi-

ant flares with luminosities of up to $10^{47}\,\mathrm{erg\,s^{-1}}$. The favoured model for these objects is a magnetar, a neutron star with an extreme magnetic field of $B \sim 10^{15}\,\mathrm{G}$. Giant flares are believed to be caused either by magnetic stresses fracturing the magnetar crust and leading to a large-scale rearrangement of the internal field (Thompson & Duncan 1995) or by a large-scale rearrangement of the magnetospheric field due to magnetic reconnection (Lyutikov 2006; Gill & Heyl 2010). The sudden release of energy and magnetic field rearrangement lead to the creation and acceleration of pair plasma that may have some baryon loading, thus leading to the emission of HENs in $p\gamma$ reactions (Halzen et al. 2005). Ioka et al. (2005) estimated the detectability of the 2004 giant flare of the Galactic SGR 1806-20 by HEN detectors. They found that detectors such as IceCube and ANTARES should detect multiple HEN events from similar Galactic SGR eruptions, provided the baryon loading is sufficiently high. The AMANDA-II detector, which was operating during the giant flare of SGR 1806-20, did not detect HENs (Achterberg et al. 2006). A search of IceCube data for HENs from regular (non-giant) Galactic SGR flares also found no significant coincident events (Abbasi et al. 2012c). Estimates based on Ioka et al. (2005) for the 5-line ANTARES detector show that, $d_{50} \approx 200\,\mathrm{kpc}$ for baryon-rich flares, suggesting that similar flares could be detected from anywhere within the Galaxy.

Significant emission of GWs in SGR giant flares may come from the potential excitation of nonradial pulsational modes with kHz-frequencies in the magnetar (de Freitas Pacheco 1998). Ioka (2001) and Corsi & Owen (2011) placed theoretical upper limits on the possible strength of the GW emission based on the energy reservoir associated with a change in the magnetic potential energy of the magnetar. They found an upper limit for the emitted GW energy of $10^{-7}\,M_\odot c^2$ to $10^{-6}\,M_\odot c^2$, which can be probed by the LIGO/Virgo network for a Galactic source (Abbott et al. 2008b; Abadie et al. 2011). However, studies that investigated the excitation of magnetar pulsational modes in more detail suggest much weaker emission that may not be detectable even with advanced-generation GW observatories (Levin & van Hoven 2011; Zink et al. 2012).

2.5. Cosmic String Kinks and Cusps

Cosmic strings are topological defects that may form in the early Universe and are predicted by grand unified theories and superstring theory (e.g., Kibble 1976; Polchinski 2004). Cosmic strings form initially as smooth loops, but through interactions and self-interactions may develop kinks and cusps (e.g., Polchinski 2004). The kinks and cusps decay, which is expected to lead to ultra-high energy cosmic ray emission with energies in excess of $\sim 10^{11}\,\mathrm{GeV}$ and up to the Planck scale (Hill et al. 1987; Bhattacharjee 1989), including ultra-high-energy neutrinos (UHENs; e.g., Anchordoqui & Halzen 2006; Berezinsky et al. 2011; Lunardini & Sabancilar 2012) and GW bursts (e.g., Damour & Vilenkin 2000; Damour & Vilenkin 2001; Mosquera Cuesta & González 2001; Siemens et al. 2006).

While not designed specifically for UHENs, HEN detectors like ANTARES and IceCube have some sensitivity to UHENs in the $\gtrsim 10^{11}\,\mathrm{GeV}$ energy range. Alvarez-Muñiz & Halzen (2001) predict, depending on details of

the underlying emission model, up to a few events per year for a km³-scale detector. Since Earth is opaque to UHENs, downgoing events must be selected. Since we are only considering ANTARES data for neutrinos that have passed through Earth (see §3.1), the present data set does not contain any potential UHEN events.

Abbasi et al. (2011a), who searched a year of IceCube-40 data for very energetic HENs, did not find neutrinos in the 10^6 GeV to 10^9 GeV energy range, but did not report limits on UHENs. A number of dedicated UHEN experiments exist, including ANITA (Gorham et al. 2010), Nu-Moon (Scholten et al. 2009) and others, but have not yet constrained many emission scenarios from cosmic strings (e.g., Lunardini & Sabancilar 2012).

The rate of GW bursts from a network of cosmic strings depends on the string tension and other network parameters, and individual bursts may be detectable with advanced detectors (Damour & Vilenkin 2001; Siemens et al. 2006). The burst shape is expected to be generic, so that matched-filtering GW analysis approaches may be employed. A first search for GW bursts from cosmic string cusps in 15 days of LIGO data from early 2005 did not reveal any candidate events (Abbott et al. 2009a).

3. GW AND HEN DETECTORS

3.1. *The* ANTARES *neutrino telescope*

Since the Earth acts as a shield against all particles except neutrinos, a neutrino telescope mainly uses the detection of upgoing muons as a signature of muon-neutrino charged-current interactions in the matter around the detector. The ANTARES detector (Astronomy with a Neutrino Telescope and Abyss environmental RESearch) is currently the only deep sea high-energy-neutrino telescope and is operating in the Northern hemisphere (Ageron et al. 2011). The telescope covers an area of about $0.1 \, \mathrm{km}^2$ on the sea bed, at a depth of 2475 m, 40 km off the coast of Toulon, France. The detector is a three-dimensional array of photomultiplier tubes (PMTs) (Aguilar et al. 2005), hosted in pressure resistant glass spheres, called optical modules (OMs) (Amram et al. 2003). In its full configuration, it is composed of 12 detection lines, each comprising up to 25 triplets of PMTs, storeys, regularly distributed along 350 m, the first storey being located 100 m above the sea bed. The first detection line was installed and connected in early 2006; the second line was put in operation in September 2006 and three more lines were connected in January 2007, so that a total of 5 lines were taking data in 2007. Five additional lines, together with an instrumentation line (containing an ensemble of oceanographic sensors dedicated to the measurement of environmental parameters), were connected by the end of 2007. The telescope reached its nominal configuration, with 12 lines immersed and taking data, in May 2008.

The three-dimensional grid of PMTs is used to measure the arrival time and position of Cherenkov photons induced by the passage of relativistic charged particles through the sea water. This information, together with the characteristic emission angle of the light (about 43 degrees), is used to determine the direction of the muon and hence infer that of the incident neutrino. The accuracy of the direction information allows to distinguish upgoing muons, produced by neutrinos, from the over-whelming background from downgoing muons, produced by cosmic ray interactions in the atmosphere above the detector (Aguilar et al. 2010). Installing the detector at great depths serves to attenuate this background and also allows to operate the PMTs in a dark environment. At high energies the large muon range makes the sensitive volume of the detector significantly greater than the instrumented volume. By searching for upgoing muons, the total ANTARES sky coverage is 3.5π sr, with most of the Galactic plane being observable and the Galactic Center being visible 70% of the sidereal day.

3.2. *Network of interferometers*

3.2.1. *LIGO*

LIGO is a network of interferometric gravitational wave detectors consisting of three interferometers in the USA. These detectors are all kilometer-scale power-recycled Michelson laser interferometers with orthogonal Fabry-Perot arms (Abbott et al. 2009b) able to detect the quadrupolar strain in space produced by the GW. Multiple reflections between mirrors located at the end points of each arm extend the effective optical length of each arm, and enhance the sensitivity of the instrument.

There are two LIGO observatories: one located at Hanford, WA and the other at Livingston, LA. The Hanford site houses two interferometers: one with 4 km arms, denoted H1, and a second with 2 km arms, denoted H2. The Livingston observatory has one 4 km interferometer, L1. The observatories are separated by a distance of 3000 km, corresponding to a time-of-flight separation of 10 ms.

The LIGO instruments are designed to detect gravitational waves with frequencies ranging from ~ 40 Hz to several kHz, with a maximum sensitivity near 150 Hz (see Fig 1). In fact, seismic noise dominates at lower frequencies and the sensitivity at intermediate frequencies is determined mainly by thermal noise, with contributions from other sources. Above ~ 200 Hz, laser shot noise corrected for the Fabry-Perot cavity response yields an effective strain noise that rises linearly with frequency. The average sensitivities of the H1 and L1 detectors during the second year of the S5 run were about 20% better than the first-year averages, while the H2 detector had about the same average sensitivity in both years.

3.2.2. *Virgo*

The Virgo detector, V1, is in Cascina near Pisa, Italy. It is a 3 km long power-recycled Michelson interferometer with orthogonal Fabry Perot arms (Accadia et al. 2012). The main instrumental difference with respect to LIGO is the seismic isolation system based on super-attenuators (Braccini et al. 2005), chains of passive attenuators capable of filtering seismic disturbances. The benefit from super-attenuators is a significant reduction of the detector noise at very low frequency (<40 Hz) where Virgo surpasses the LIGO sensitivity. During 2007, above 300 Hz, the Virgo detector had sensitivity similar to the LIGO 4 km interferometers, while above 500 Hz it is dominated by shot noise, see Fig 1.

The time-of-flight separation between the Virgo and Hanford observatories is 27 ms, and 25 ms between Virgo and Livingston. Due to the different orientation of its arms, the angular sensitivity of Virgo is complementary to that of the LIGO detectors, Virgo therefore

enhances the sky coverage of the network. Moreover, simultaneous observations of multiple detectors are crucial to reject environmental and instrumental effects.

At the time of writing the LIGO and Virgo interferometers are undergoing upgrades to "advanced" configurations with distance sensitivity improved by approximately a factor of 10 (Harry et al. 2010). The advanced instruments will commence operations around 2015.
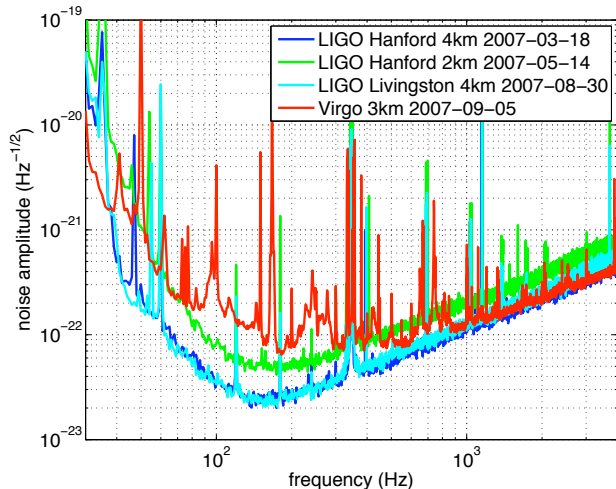

Fig. 1.— Noise amplitude spectral densities of the four LIGO and Virgo detectors during S5.

3.3. Joint data taking periods

The fifth LIGO science run, S5 (Abbott et al. 2008a), was held from 2005 November 4 to 2007 October 1. Over one year of science-quality data were collected with all three LIGO interferometers in simultaneous operation at their design sensitivity, with duty factors of 75%, 76%, and 65% for H1, H2, and L1. The Virgo detector started its first science run, VSR1 (Acernese et al. 2008), on 2007 May 18. The Virgo duty factor over VSR1 was 78%. During this period, ANTARES was operating in its 5 line configuration. The concomitant set of ANTARES 5-line (5L), VSR1 and S5 data covers the period between January 27 and September 30, 2007; these data are the subject of the analysis presented here.

4. SELECTION OF HEN CANDIDATES

4.1. HEN data sample

The ANTARES data sample used in the analysis is composed of runs from 2007 selected according to various quality criteria, based mainly on environmental parameters (e.g. sea current, counting rates), configuration and behaviour of the detector during the given run (e.g. duration of the run, alignment of the detector). Two basic quantities are used to characterise the counting rate of a given OM: the baseline rate (^{40}K activity and bioluminescence) and the burst fraction (flashes of light emitted by marine organisms). The baseline rate represents the most probable counting rate of a given OM computed from the rate distributions in each PMT over the whole run (typically a few hours). The burst fraction corresponds to the fraction of time during which the

OM counting rates exceed by more than 20% the estimated baseline. The data selected for this search are required to have a baseline rate below 120 kHz and a burst fraction lower than 40%, with 80% of all OMs being active. With these quality criteria, the active time is 103.4 days out of the 244.8 days of the 5-line period. Finally, when restricting the data to the concomitant period with LIGO/Virgo, the remaining equivalent time of observation is $T_{obs} = 91$ days.

4.2. Trigger levels

The ANTARES trigger system is multi-level (Aguilar et al. 2007). The first level is applied in situ, while the remaining levels intervene after all data are sent to the shore station and before being written on disk. Trigger decisions are based on calculations done at three levels. The first trigger level, L0, is a simple threshold of about 0.3 photo-electron (pe) equivalent charge applied to the analog signal of the PMT. The second level trigger, L1, is based on two coincident L0 hits in the same storey within 20 ns or hits with large charge ($\geq$ 3 pe or 10 pe depending on the configuration). The L2 trigger requires the presence of at least five L1 hits in a 2.2 μs time window (roughly the maximum muon transit time across the detector) and that each pair of L1 hits are causally related according to the following condition: $\Delta t_{ij} \leq d_{ij}n/c + 20$ ns. Here Δt_{ij} and d_{ij} are the time difference and distance between hits i and j, c is the speed of light in vacuum and n is the index of refraction.

4.3. Reconstruction strategy

Hits selected according to the criteria described in Section 4.2 are then combined to reconstruct tracks using their arrival time and charge as measured by the corresponding OM. Muons are assumed to cross the detector at the speed of light along a straight line from which the induced Cherenkov light originates. The time and charge information of the hits in the PMTs is used in a minimisation procedure to obtain the track parameters, namely, its direction (θ, ϕ) and the position (x_0, y_0, z_0) of one track point at a given time t_0. The reconstruction algorithm used for this analysis is a fast and robust method (Aguilar et al. 2011b) which was primarily designed to be used on-line.

4.3.1. Description of the algorithm

The algorithm is based on a χ^2-minimisation approach. Its strict hit selection leads to a high purity up-down separation while keeping a good efficiency. The exact geometry of the detector is ignored: the detector lines are treated as straight and the 3 OMs of each storey are considered as a single OM centered on the line. Thus, the hit's altitude corresponds to the optical modules altitude. All hits at the same floor in coincidence within 20 ns are merged into one hit. The time of the merged hit is that of the earliest hit in the group and its charge is the sum of the charges. The algorithm uses the L1 hits as a seed for the hit selection. It requests a coincidence of 2 L1 hits in two adjacent floors within 80 ns or 160 ns in two next-to-adjacent floors. The quality of the reconstruction is measured by a χ^2-like variable with NDF degrees of freedom, based on the time differences between the hit times t_i and the expected arrival time t_i^γ of photons from

the track or bright-point (see Section 4.4). The quality function is then extended with a term that accounts for measured hit charges q_i and the calculated photon travel distances d_i^γ:

$$\chi^2 = \frac{1}{NDF} \sum_{i=1}^{N_{\text{hit}}} \left[\frac{\Delta t_i^2}{\sigma_i^2} + \frac{Q(q_i)}{\bar{q}} \frac{D(d_i^\gamma)}{d_0} \right]. \qquad (1)$$

In this expression, σ_i is the timing error, set to $10\,\text{ns}$ for charges larger than $2.5\,\text{pe}$ and to $20\,\text{ns}$ otherwise. $\Delta t_i = t_i^\gamma - t_i$ is the time residuals between the hit time t_i and the expected arrival time of the photons t_i^γ from the muon track. In the second term, $\bar{q}$ is the average hit charge calculated from all hits which have been selected for the fit and $d_0 = 50\,\text{m}$ is the typical distance at which the signal in one PMT from a Cherenkov light front is of the order of 1 pe. The function $Q(q_i)$ accounts for the angular acceptance of the OMs, while $D(d_i^\gamma)$ penalises large amplitude hits originating from large distance tracks. A proper cut on the fit quality parameter allows the isolation of a high purity neutrino sample, which is crucial in the subsequent analysis.

4.3.2. Azimuthal degeneracy of the reconstruction

For a particle trajectory reconstructed from a Cherenkov cone giving hits on only two straight detector lines, there always exists an alternative trajectory having an identical χ^2 value, but a different direction. The degenerate trajectory is the mirror image of the original track in the plane formed by the two lines. As a consequence, each event reconstructed with only two lines will have two equiprobable arrival directions, which must be taken into account during the subsequent GW analysis.

4.4. Criteria for HEN event selection

The initial sample of reconstructed events contains both upgoing neutrino induced muons and downgoing muons from cosmic ray interactions in the atmosphere. Some of the atmospheric muons are misreconstructed as upgoing and the selection cuts, based on Monte-Carlo simulations, are devised to reduce this contamination so as to maximise the discovery potential. A minimum of 6 hits on at least 2 lines are required to reconstruct a track. Only upgoing tracks are kept for further analysis. Quality cuts are then applied based on two quantities computed according to equation (1). The first parameter used, χ_t^2, is the quality factor associated with the reconstructed particle track, whereas the second one, χ_b^2, is associated with a bright-point, light emitted from a point-like source inside the detector. This rejects events from large electromagnetic showers, likely to appear in downgoing muon bundles for instance.

A cut on χ_b^2 reduces the number of such events and decreases the contribution of misreconstructed muons in the background. Further cuts are applied on χ_t^2 depending on the arrival direction of the candidate - the muon contamination increases close to the horizon - which reduce the fraction of misreconstructed muons to less than 20% over the whole sample, while optimising the sensitivity (see Section 4.6 and Halladjian (2010)).

Figure 2 shows the distribution of the sine of the declination of the events selected with the final cuts, which is globally consistent with background.
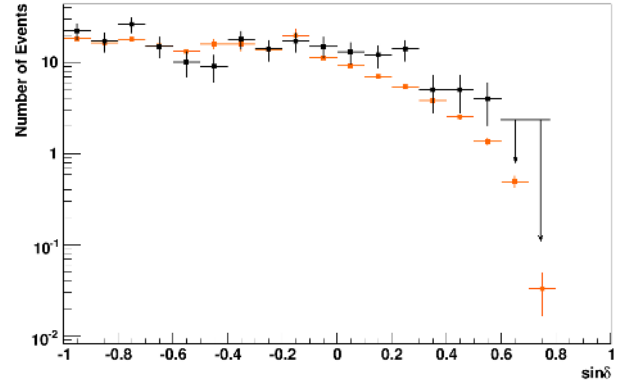

FIG. 2.— Distribution of the sine of the declination δ of selected events (black points), compared to Monte-Carlo expectations (sum of atmospheric muons and atmospheric neutrinos, orange (or grey) points).

4.5. Angular error

The distribution of the space angle Ω between the true neutrino arrival direction and the reconstructed muon track can be described by a log-normal distribution:

$$P(\Omega) = \frac{1}{\sqrt{2\pi}} \frac{e^{-\frac{1}{2\sigma_0^2}\left(\ln\left(\frac{\Omega - \theta_0}{m_0}\right)\right)^2}}{(\Omega - \theta_0)\,\sigma_0}, \qquad (2)$$

where θ_0 is a location parameter, σ_0 is related to the shape of the distribution and m_0 is a scaling parameter. In all cases for our study, the location parameter θ_0 is close to zero, and $(\Omega - \theta_0) > 0$ is always satisfied. This distribution depends on the energy associated to the track (estimated through the number of photons detected) and its declination. This parametrisation is used during the GW search to compute the significance of a hypothetical signal for the scanned directions inside the angular search window centred around the reconstructed neutrino arrival direction. Figure 3 shows an example of distribution of the space angle for a sample of Monte Carlo neutrinos with an E^{-2} spectrum, together with the best-fit parametrisation and the 50th and 90th percentiles of the distribution.

One of the main variables to describe the performance of a neutrino telescope is the angular resolution, defined as the median of the distribution of the angle between the true neutrino direction and the reconstructed track, also indicated in Figure 3. This number is estimated from simulations.

For those events of our selected sample reconstructed with at least three lines the angular resolution is, assuming an E^{-2} energy spectrum, $\sim 2.5°$ at $100\,\text{GeV}$, improving to $1°$ around $100\,\text{TeV}$. For 2-line events, when selecting the reconstructed track closer to the true direction, the angular accuracy varies between $3°$ at low energy ($100\,\text{GeV}$) and $2.5°$ at high energy ($100\,\text{TeV}$).

We define the angular search window for the GW analysis as the 90th percentile of the distribution, also indicated in Figure 3; this window lies between $5°$ and $10°$ for 3-line events, depending on declination, and between $10°$ and $15°$ for 2-line events.

We note that the typical angular distance between galaxies within $10\,\text{Mpc}$ is a few degrees (White et al.
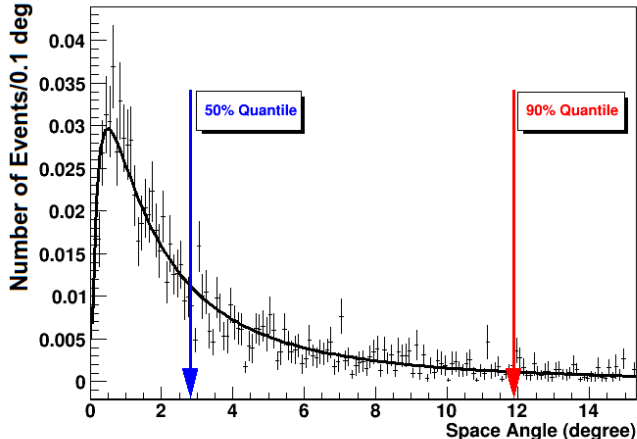
FIG. 3.— Example of space angle distribution with the associated fit to equation (2) obtained with a sample of Monte-Carlo HEN events, for a given declination and a given number of hits. The arrows indicate the 50th (median) and the 90th percentiles of the distribution. The distribution is normalised to unity.

2011), much smaller than the typical size of the 90th percentile error region for our HEN events. This implies that we can associate a potential host galaxy to any of the HEN candidates if it turns out to be of cosmic origin.

4.6. Analysis sensitivity and selected HEN candidates

The limit-setting potential of the analysis, or sensitivity, has been quantified for the whole 5 line data period. Specifically, the sensitivity is defined as the median 90% upper limit obtained over an ensemble of simulated experiments with no true signal. The sensitivity depends on the declination of the potential source. For our sample and assuming an E^{-2} steady flux, using the selection criteria described, the best sensitivity has been estimated to be $E^2 \frac{dN}{dE} \approx 10^{-6}\,\text{GeV}\,\text{cm}^{-2}\,\text{s}^{-1}$. This best sensitivity is reached below $-47°$; i.e., at declinations which are always below the horizon at the latitude of ANTARES ($43°\text{N}$).

With the selection previously described, 181 runs corresponding to 104 days of live time were kept for the analysis. The selection has been divided into events reconstructed with 2 lines and events with at least 3 lines. Each of the mirror solutions for 2 line events will be searched for possible counterparts in the subsequent GW analysis. This results in 216 neutrinos to be analysed: 198 with two possible directions and 18 reconstructed with at least 3 lines. Figure 4 is a sky map of the candidate HEN events, where the degenerate solutions for 2 line events can be seen.

Of these HEN events, 158 occurred at times when at least two gravitational-wave detectors were operating. Since two or more detectors are required to discriminate GW signals from background noise (as described in Section 5.2), in the following we consider only these remaining 158 HEN candidates: 144 2-line events and 14 3-line events[149].

---

[149] Details of each of the HEN candidate events are given at https://dcc.ligo.org/cgi-bin/DocDB/ShowDocument?docid=p1200006.

Finally, we note that IceCube operated in its 22-string configuration for part of 2007 (Abbasi et al. 2012c). However, this data was only used for time-dependent searches applied to source directions with observed X-ray or gamma-ray emission, such as GRBs; there were no untriggered, time-dependent searches over the sky. Furthermore, a comparison of ANTARES and IceCube sensitivities in 2007 indicates that the bulk of our HEN neutrino triggers come from declinations (the southern sky) such that it is unlikely that IceCube could have detected the source independently.

5. GW SEARCH METHOD

5.1. Search procedure

One of the simplest searches that may be performed combining GW and HEN data is a triggered analysis that scans GW data around the time of the putative neutrino event by cross-correlating data from pairs of detectors. This search exploits knowledge of the time and direction of the neutrino event to improve the GW search sensitivity. We use the X-PIPELINE algorithm (Sutton et al. 2010), which has been used in similar searches for GWs associated with GRBs (Abbott et al. 2010; Abadie et al. 2012b). X-PIPELINE performs a coherent analysis of data from arbitrary networks of gravitational wave detectors, while being robust against background noise fluctuations. Each trigger is analysed independently of the others, with the analysis parameters optimised based on background noise characteristics and detector performance at the time of that trigger, thereby maximising the search sensitivity.

5.2. GW event analysis

In our GW search, a neutrino candidate event is characterised by its arrival time, direction, and angular search window (and mirror-image window, for the 2-line events). Also important is the range of possible time delays (both positive and negative) between the neutrino emission and the associated gravitational-wave emission. This quantity is referred to as the *on-source* window for the neutrino; it is the time interval which is searched for GW signals. We use a symmetric on-source window of $\pm 496\,\text{s}$ (Baret et al. 2011), which is conservative enough to encompass most theoretical models of GW and HEN emission. The maximum expected time delay between GWs and HENs due to a non-zero mass effect for either particle is much smaller than the coincidence windows used.

The basic search procedure follows that used in Abbott et al. (2010). All detectors operating at the time of the trigger and which pass data-quality requirements are used for the GW search. The data from each detector are first whitened and time-delayed according to the sky location being analysed so that a GW signal from that direction would appear simultaneous in each data stream. The data are then Fourier transformed to produce time-frequency maps. The maps are summed coherently (using amplitude and phase) with weighting determined by each detector's frequency-dependent sensitivity and response to the sky location in question; the weightings are chosen to maximise the signal-to-noise ratio expected for a circularly polarized GW signal[150], which is

---

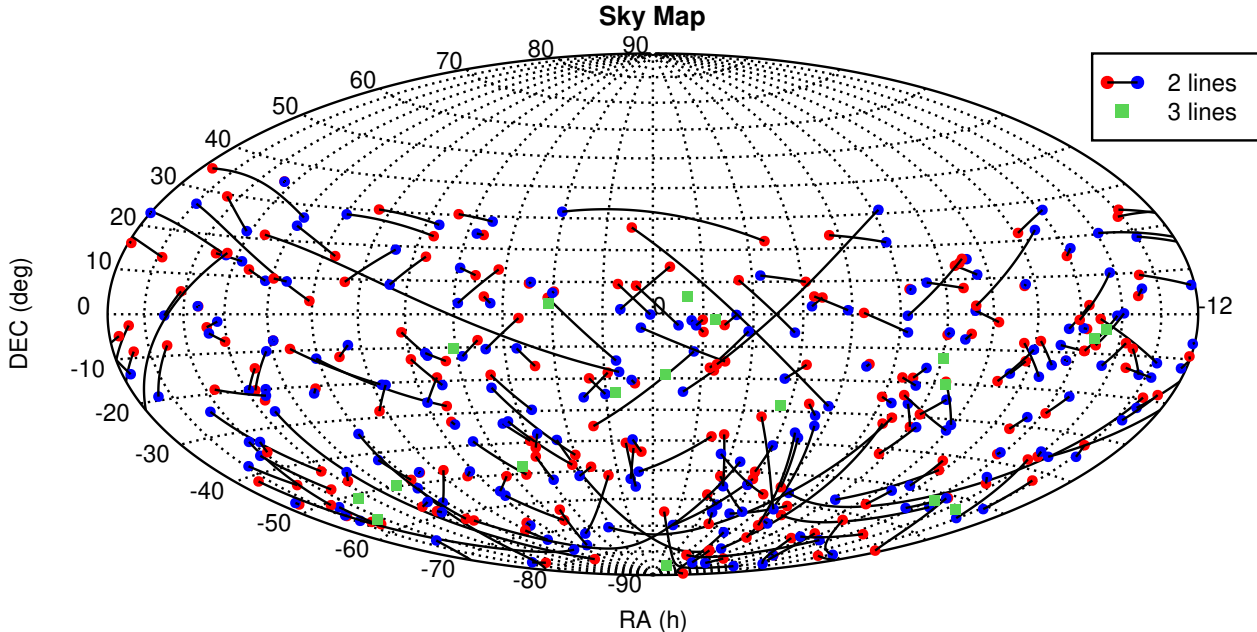[150] Empirically it is found that the circular polarisation re-

Sky Map

FIG. 4.— Skymap of the selected 216 HEN events in equatorial coordinates. A line connects the associated mirror solutions for events reconstructed with two lines as described in Section 4.3.2.

the expected polarisation for a GW source observed from near the rotational axis (Kobayashi & Meszaros 2003). A threshold is placed on the map to retain the largest 1% of pixels by energy (squared amplitude). Surviving pixels are grouped using next-nearest-neighbours clustering; each cluster of pixels is considered as a candidate GW event. The event cluster is assigned a combined energy by summing the energy values of its constituent pixels; this combined energy is used as the ranking statistic for the events.

In addition to the marginalised circular polarization sum, a second ranking statistic is computed based on a maximum-likelihood analysis of the event assuming power-law distributed background noise with no assumption on the GW polarization. In practice this statistic is often found to provide signal-noise separation due to the non-Gaussian nature of the GW detector noise. Other combinations of the data are also constructed. Of particular importance are "null" combinations designed to cancel out the GW signal from the given sky location; comparison to corresponding "incoherent" combinations provides powerful tests for identifying events due to background noise fluctuations (Chatterji et al. 2006), and are described in detail in Was et al. (2012). Events are also characterised by their duration, central time, bandwidth, and central frequency.

The time-frequency analysis is repeated for Fourier transform lengths of 1/128, 1/64, 1/32, 1/16, 1/8, 1/4 s, to maximise the sensitivity to GW signals of different durations. It is also repeated over a grid of sky positions covering the 90% containment region of the HEN. This grid is designed such that the maximum relative timing error between any pair of GW detectors is less that 0.5 ms. When GW events from different Fourier transforms lengths or sky positions overlap in time-frequency,

the highest-ranked event is kept and the others discarded. Finally, the events are decimated to a rate of 0.25 Hz before being written to disk.

This time-frequency analysis is performed for all of the data in the ± 496 s on-source window. To estimate the significance of the resulting GW candidates, the same analysis is repeated for all coincident data in the *off-source* window, defined as all data within ± 1.5 hours of the neutrino time, excluding the on-source interval. The same set of detectors and data-quality requirements as in the on-source analysis are used for the off-source data. These off-source data provide a sample of background that does not contain any signal associated with the neutrino event, but with statistical features similar to the data searched in association with the neutrino. To enlarge the background sample, we also repeat the off-source analysis after applying time shifts of multiples of 6 s to the data from one or more detectors; with such time slides we were able to produce $O(10^3)$ background trials for each HEN.

Finally, the analysis is repeated after "injecting" (adding) simulated GW signals to the on-source data. The amplitudes and morphologies tested are discussed in Section 6.3.1. We use these simulations to optimise and assess the sensitivity of the search, as discussed below.

5.3. *GW search optimisation*

The sensitivity of searches for gravitational-wave bursts tends to be limited by the presence of non-Gaussian fluctuations of the background noise, known as glitches. To reduce this background, events that overlap in time within known instrumental and/or environmental disturbances are discarded. In addition to this "veto" step, GW consistency tests comparing the coherent and incoherent energies are applied to each event (Was et al. 2012). These tests are applied to the on-source, off-source and injection events; events failing one

striction also improves the overall detection probability for *linearly* polarised GWs, as the resulting background reduction outweighs the impact of rejecting some linearly polarised GWs.

or more of these tests are discarded. The thresholds are optimised by testing a preset range of thresholds and selecting those which give the best overall detection efficiency at a fixed false alarm probability of 1% when applied to a random sample of background and injection events (the on-source events are *not* used; i.e., this is a blind analysis). These tests also determine which of the two ranking statistics discussed in Section 5.2 (based on circularly polarized GW energy or powerlaw noise) gives the better detection efficiency; the winner is selected as the final ranking statistic.

Once the thresholds have been fixed, these consistency tests are applied to the on-source events and to the remaining off-source and injection events (those not used for tuning). The surviving on-source event with the largest significance (highest energy or powerlaw statistic) is taken to be the best candidate for a gravitational wave signal and is referred to as the loudest event (Brady et al. 2004). All surviving on-source events are assigned a false alarm probability by comparison to the distribution of loudest events from the off-source trials. Any on-source event with probability $p < 0.01$ is subjected to additional checks to try to determine the origin of the event and additional background time slide trials are performed to improve the accuracy of the false alarm probability estimate.

After the p values have been determined for the loudest events associated with each of the 158 HEN events, the collective set of p values is tested for consistency with the null hypothesis (no GW signal) using the binomial test, discussed in Section 6.2. We also set a frequentist upper limit on the strength of gravitational waves associated with each neutrino trigger, as discussed in Section 6.3.

5.4. *Low-frequency and high-frequency GW analyses*

Given our knowledge of possible GW sources discussed in Section 2, the most likely detectable signals at extragalactic distances are in the low-frequency band ($f \lesssim 500 \, \text{Hz}$), where our detectors have maximum sensitivity, see Fig 1. At the same time, the computational cost of the X-PIPELINE analysis increases at high frequencies. This is due in part to the extra data to be analysed, but also to the need for finer-resolution sky grids to keep time delay errors much smaller than one GW period. We therefore split the gravitational wave band into two regions: $60 \, \text{Hz}$ to $500 \, \text{Hz}$ and $500 \, \text{Hz}$ to $2000 \, \text{Hz}$. The low-frequency band is analysed for all HEN events – such a search is computationally feasible while covering the highest-sensitivity region of the GW detectors. However, compact objects such as neutron stars or collapsar cores have characteristic frequencies for GW emission above $500 \, \text{Hz}$. Such emissions might be detectable from Galactic sources such as soft gamma repeater giant flares, or possibly from nearby galaxies. Since the computational cost of a high-frequency search for all HEN events is prohibitive with the current analysis pipeline, we perform the $500 \, \text{Hz}$ to $2000 \, \text{Hz}$ analysis on the 3-line HEN events only. The 3-line events are a small subset ($\sim 10\%$) of the total trigger list and have the smallest sky position uncertainties, and therefore the smallest computational cost for processing. To reduce the computational cost further, we use the same sky grid for the high-frequency search as was used at low frequencies, after determining that the loss of sensitivity is acceptable.

The high-frequency analysis is performed independently of the low-frequency analysis (independent tuning, background estimation, etc.) using the identical automated procedure. In the following sections we will present the results of the low- frequency and high-frequency searches separately.

6. COINCIDENT SEARCH RESULTS

6.1. *Per-HEN GW candidates*

We analysed GW data in coincidence with 158 neutrino candidates for the low frequency search, and 14 neutrino events for the high frequency search. In the low frequency analysis, only one neutrino trigger had a corresponding GW event with false alarm probability below the threshold of $p = 0.01$ to become a candidate event. We found no candidates in the high frequency search. For the low-frequency candidate, additional time shifts totaling 18064 background trials yielded a refined false alarm probability of $p = 0.004$, which is not significant given a trials factor of 158 (this statement is quantified below). This event came from analysis of the H1, H2, and V1 data; follow-up checks were performed, including checks of detector performance at the time as indicated by monitoring programs and operator logs, and scans of data from detector and environmental monitoring equipment to look for anomalous behaviour. While these checks did not uncover a physical cause for the event, they did reveal that it occurred during a glitching period in V1. We conclude that we have no clear gravitational wave burst signal associated with any of our sample of 158 neutrino events.

6.2. *Search for a cumulative excess: binomial test*

A quantitative analysis of the significance of any candidate gravitational-wave event must take account of the trials factor due to the number of neutrino events analysed. We use the binomial test, which has been applied in previous GRB-triggered GW searches (Abbott et al. 2008c, 2010). Under the null hypothesis, the false alarm probabilities p for each HEN loudest event are expected to be uniformly distributed between 0 and 1. The binomial test compares the measured p values to the null distribution to determine if there is a statistically significant excess of (one or more) small p values which may be due to gravitational wave signals.

Briefly, the binomial test sorts the set of N measured loudest event probabilities in ascending order: $p_1 \leq p_2 \leq p_3 \leq ... \leq p_N$. For each $i \in [1, N_{\text{tail}}]$ we compute the binomial probability $P_{\geq i}(p_i)$ of getting i or more events with p values $\leq p_i$:

$$P_{\geq i}(p_i) = \sum_{k=i}^{N} \frac{N!}{(N-k)!k!} p_i^k (1 - p_i)^{N-k} \, . \qquad (3)$$

Here N is the number of HEN events analysed (158 in the $60 \, \text{Hz}$ to $500 \, \text{Hz}$ band and 14 in the $500 \, \text{Hz}$ to $2000 \, \text{Hz}$ band), and N_{tail} is the number of the smallest p values we wish to test. We choose N_{tail} to be 5% of N; i.e., $N_{\text{tail}} = 8$ for the low frequency band and $N_{\text{tail}} = 1$ for the high frequency band.

The lowest $P_{\geq i}(p_i)$ for $i \in [1, N_{\text{tail}}]$ is taken as the most significant deviation from the null hypothesis. To assess the significance of the deviation, we repeat the test using

p values drawn from a uniform distribution and count the fraction of such trials which give a lowest $P_{\geq i}(p_i)$ smaller than that computed from the true measured p values.

Figures 5 and 6 show the cumulative distribution of p values measured in the low- and high-frequency analyses. In both cases the measured p values are consistent with the null hypothesis.
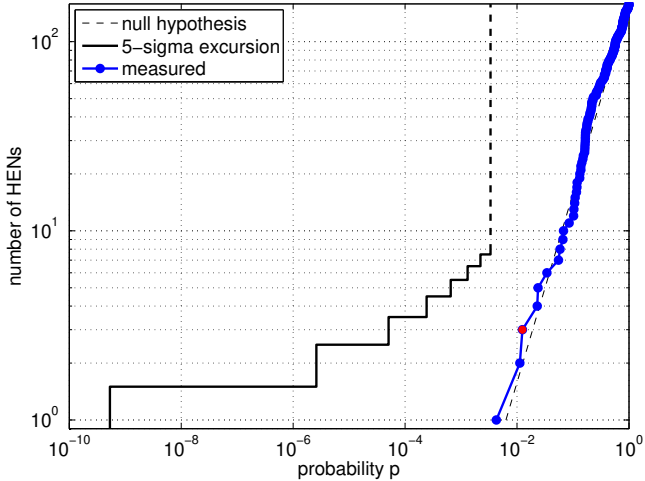

FIG. 5.— Distribution of observed p values for the loudest GW event associated with each neutrino analysed in the low frequency analysis. The red dot indicates the largest deviation of the low p tail from the uniform distribution null hypothesis; this occurs due to having the three loudest events below $p_3 \sim 0.013$. Deviations this large or larger occur in approximately 64% of experiments under the null hypothesis. The black line shows the threshold for a 5-sigma deviation from the null hypothesis.
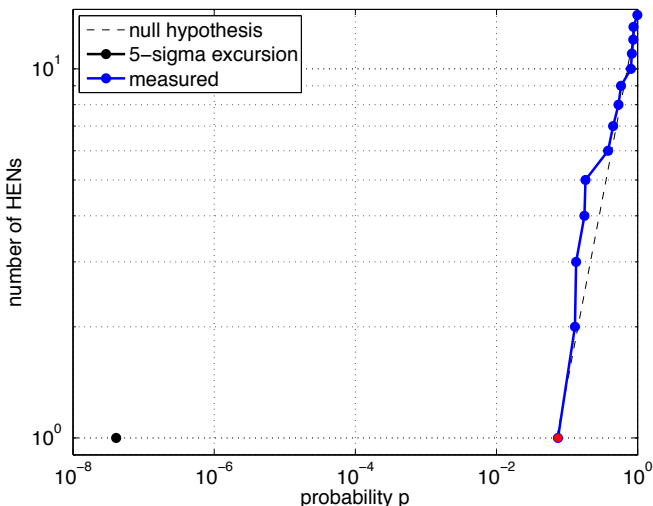
FIG. 6.— Distribution of observed p values for the loudest GW event associated with each neutrino analysed in the high frequency analysis. The red dot indicates the largest deviation of the low p tail from the uniform distribution null hypothesis; since $N_{\text{tail}} = 1$, this is constrained to occur for p_1. Deviations this large or larger occur in approximately 66% of experiments under the null hypothesis. The black dot shows the threshold for a 5-sigma deviation from the null hypothesis.

6.3. GW upper limits

The sensitivity of the GW search is determined by a Monte-Carlo analysis. For each neutrino trigger, we add simulated GW signals to the on-source data and repeat the analysis described in Section 5.2. We consider a simulated signal detected if it produces an event louder than the loudest on-source event after all event tests have been applied. We define a 90% confidence level lower limit on the distance to the source as the maximum distance $D_{90\%}$ such that for any distance $D \leq D_{90\%}$ the probability of detection is 0.9 or greater.

6.3.1. Injected waveforms

As in GRB-triggered searches, we use a mix of ad hoc and astrophysically motivated GW waveforms. The ad hoc waveforms are Gaussian-modulated sinusoids:

$$h_+ = \frac{(1 + \cos^2 \iota)}{2} \frac{h_{\text{rss}}}{(2\pi\tau^2)^{\frac{1}{4}}} e^{-\frac{(t-t_0)^2}{4\tau^2}} \cos 2\pi f_0(t - t_0) , \quad (4)$$

$$h_\times = \cos \iota \frac{h_{\text{rss}}}{(2\pi\tau^2)^{\frac{1}{4}}} e^{-\frac{(t-t_0)^2}{4\tau^2}} \sin 2\pi f_0(t - t_0) . \quad (5)$$

Here f_0 is the central frequency, t_0 is the central time, and τ is the duration parameter. This waveform is consistent with the GW emission from a rotating system viewed from an inclination angle ι to the rotational axis. We select the inclination uniformly in $\cos \iota$ with $\iota \in [0°, 5°]$. This corresponds to a nearly on-axis system, such as would be expected for association with an observed long GRB. We chose $\tau = 1/f_0$, and use central frequencies of $100\,\text{Hz}$, $150\,\text{Hz}$, and $300\,\text{Hz}$ for the low-frequency analysis and $554\,\text{Hz}$ and $1000\,\text{Hz}$ for the high-frequency search. The quantity h_{rss} is the root-sum-square signal amplitude:

$$h_{\text{rss}} \equiv \sqrt{\int \left(h_+^2(t) + h_\times^2(t) \right) dt} . \quad (6)$$

For the small values of ι considered here ($\iota < 5°$) this amplitude is related to the total energy E_{GW} in a narrow-band gravitational-wave burst by

$$E_{\text{GW}} \simeq \frac{2}{5} \frac{\pi^2 c^3}{G} h_{\text{rss}}^2 f_0^2 D^2 . \quad (7)$$

For astrophysical injections we use the gravitational-wave emission of inspiraling neutron star and black hole binaries, which are widely thought to be the progenitors of short GRBs. Specifically, we use the post-Newtonian model for the inspiral of a double neutron star system with component masses $m_1 = m_2 = 1.35M_\odot$, and the one for a black-hole - neutron-star system with $m_1 = 5M_\odot$, $m_2 = 1.35M_\odot$. We set the component spins to zero in each case. Motivated by estimates of the jet opening angle for short GRBs, we select the inclination uniformly in $\cos \iota$ with $\iota \in [0°, 30°]$.

For each HEN trigger, the injections are distributed uniformly in time over the on-source window. The injection sky positions are selected randomly following the estimated probability distribution (2) for the HEN trigger, to account for the uncertainty in the true HEN direction of incidence. The polarization angle (orientation of the rotational axis on the sky) is distributed uniformly. Finally, the amplitude and arrival time at each detector is

perturbed randomly to simulate the effect of calibration errors in the LIGO and Virgo detectors.

6.3.2. *Exclusion distances*

For each waveform type we set a 90% confidence level lower limit on the distance to a GW source associated with a given HEN trigger[151]. This is defined as the maximum distance $D_{90\%}$ such that for any distance $D \leq D_{90\%}$ there is a probability of at least 0.9 that such a GW signal would have produced an event louder than the loudest on-source event actually measured. For inspirals, each distance corresponds to a well-defined amplitude. We can associate an amplitude to each distance for the sine-Gaussian waveforms as well, by assuming a fixed energy in gravitational waves. For concreteness, we select $E_{\mathrm{GW}} = 10^{-2} M_\odot c^2$. This corresponds to the optimistic limit of possible gravitational-wave emission by various processes in the collapsing cores of rapidly rotating massive stars (Fryer et al. 2002; Kobayashi & Mészáros 2003; Piro & Pfahl 2007; Fryer & New 2011, and discussion in Sec. 2); more conservative estimates based on simulations have been made in Dimmelmeier et al. (2008); Ott (2009); Scheidegger et al. (2010); Ott et al. (2011); Takiwaki & Kotake (2011).

For each type of gravitational wave simulated, the distributions of exclusion distances for our neutrino sample are shown in Figures 7 and 8. For binary neutron star systems of $(1.35 - 1.35)M_\odot$ and black hole - neutron star systems of $(5 - 1.35)M_\odot$ typical distance limits are 5 Mpc and 10 Mpc respectively. For the sine-Gaussian waveforms with $E_{\mathrm{GW}} = 10^{-2} M_\odot c^2$ we find typical distance limits between 5 Mpc and 17 Mpc in the low-frequency band and of order 1 Mpc in the high-frequency band. For other E_{GW} the limits scale as $D_{90\%} \propto (E_{\mathrm{GW}}/10^{-2} M_\odot c^2)^{1/2}$. For example, for $E_{\mathrm{GW}} = 10^{-8} M_\odot c^2$ (typical of core-collapse supernovae) a signal would only be observable from a Galactic source.

7. ASTROPHYSICAL IMPLICATIONS

Observational constraints on joint sources of GW and HEN signals have been derived in Bartos et al. (2011). However, they are based on the interpretation and the combination of previously published and independent GW and HEN observational results. The results presented in this section are the first derived from a joint GW-HEN analysis, using concomitant data obtained with LIGO/Virgo and ANTARES.

7.1. *Upper limits on GW-HEN populations*

The present search for GW and HEN correlations in space and time revealed no evidence for coincident events. This implies a 90% confidence level upper limit on the rate of detectable coincidences of $2.3/T_{\mathrm{obs}}$, where $T_{\mathrm{obs}} \approx 90$ days is the duration of coincident observations. This can be expressed as a limit on the rate density (number per unit time per unit volume) $\rho_{\mathrm{GW\text{-}HEN}}$ of joint GW-HEN sources:

$$\rho_{\mathrm{GW\text{-}HEN}} \leq \frac{2.3\mathcal{F}_b}{VT_{\mathrm{obs}}}. \qquad (8)$$

[151] Upper limits for each waveform and HEN trigger are available at https://dcc.ligo.org/cgi-bin/DocDB/ShowDocument?docid=p1200006.
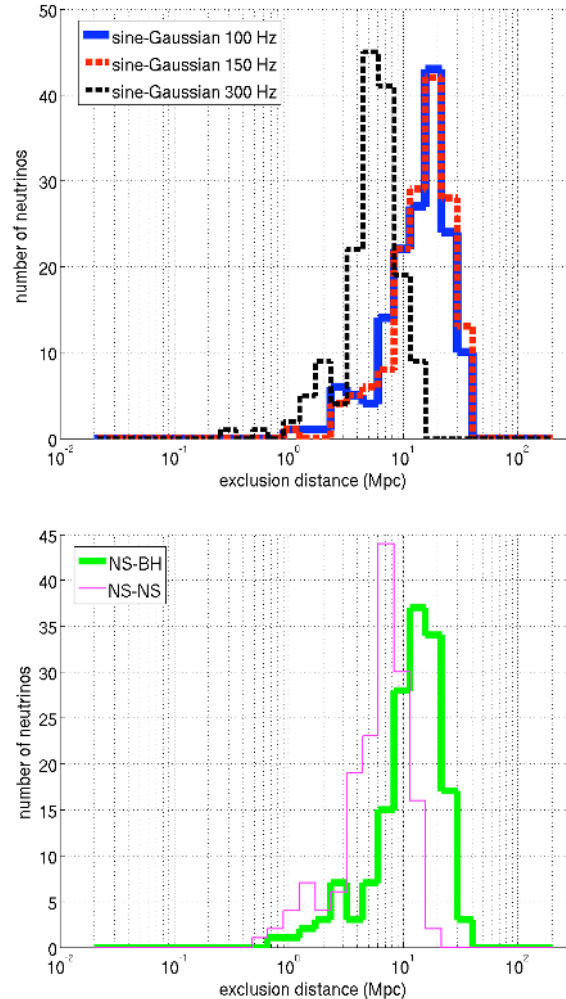

FIG. 7.— Low-frequency analysis: the top plot is the histogram for the sample of analysed neutrinos of the distance exclusions at the 90% confidence level for the 3 types of sine-Gaussian models considered: 100 Hz, 150 Hz and 300 Hz. A standard siren gravitational wave emission of $E_{GW} = 10^{-2} M_\odot c^2$ is assumed. The bottom plot shows the distance exclusions for the 2 families of binary inspiral models considered: NS-NS and BH-NS.

Here $\mathcal{F}_b$ is the beaming factor (the ratio of the total number of sources to the number with jets oriented towards Earth[152]), and V is the volume of universe probed by the present analysis for typical GW-HEN sources.

We take as fiducial sources two classes of objects: the final merger phase of the coalescence of two compact objects (short GRB-like), or the collapse of a massive object (long GRB-like), both followed by the emission of a relativistic hadronic jet. We define the HEN horizon as the distance for which the probability to detect at least 1 HEN in ANTARES with 5 lines is 50%. In the case of short GRBs (SGRBs), the HEN horizon is estimated to be $d_{50} = 4$ Mpc using Guetta et al. (2004), while the typical GW horizon from the inspiral model is 5 Mpc to 10 Mpc depending on the binary masses. For long GRBs (LGRB) the HEN horizon increases to $d_{50} = 12$ Mpc using Guetta et al. (2004). The GW emission associated with long GRBs is highly uncertain; our optimistic

[152] For example, for a jet opening angle of 5° gives $\mathcal{F}_b \sim 300$, while 30° gives $\mathcal{F}_b \sim 10$.
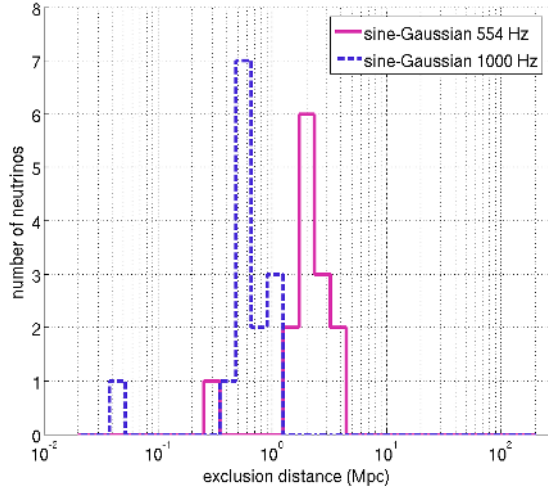
tance.

Fig. 8.— High-frequency analysis: the histogram for the sample of analysed neutrinos of the distance exclusions at the 90% confidence level for the 2 frequencies of circular sine-Gaussian models considered: $554\,\mathrm{Hz}$ and $1000\,\mathrm{Hz}$.

assumption of $E_{\mathrm{GW}} = 10^{-2} M_\odot c^2$ at low frequencies gives a typical horizon distance of $10\,\mathrm{Mpc}$ to $20\,\mathrm{Mpc}$ in GW. Using the lower of the GW and HEN distances in each case yields from equation (8) approximate limits on the population density. For SGRB-like sources, related to the merger of two compact objects, we find $\rho_{\mathrm{GW\text{-}HEN}}^{\mathrm{SGRB}} \lesssim \mathcal{F}_b \times 10^{-2}\,\mathrm{Mpc}^{-3}\,\mathrm{yr}^{-1}$. For LGRB-like sources, related to the collapse of massive stars, we find $\rho_{\mathrm{GW\text{-}HEN}}^{\mathrm{LGRB}} \lesssim \mathcal{F}_b E_{0.01}^{-3/2} \times 10^{-3}\,\mathrm{Mpc}^{-3}\,\mathrm{yr}^{-1}$, where $E_{0.01} \equiv E_{\mathrm{GW}}/10^{-2} M_\odot c^2$.

7.2. Comparison of limits with existing estimates

Guetta & Piran (2006), Nakar et al. (2006), and Guetta & Stella (2009) suggest a local rate density of SGRBs of $\rho_{\mathrm{SGRB}} \sim 10^{-7}\,\mathrm{Mpc}^{-3}\,\mathrm{yr}^{-1}$ to $10^{-6}\,\mathrm{Mpc}^{-3}\,\mathrm{yr}^{-1}$ after correcting for beaming effects. This is similar to the abundance of binary neutron star mergers, their assumed progenitors, estimated to be $\rho_{\mathrm{NS\text{-}NS}} \sim 10^{-8}\,\mathrm{Mpc}^{-3}\,\mathrm{yr}^{-1}$ to $10^{-5}\,\mathrm{Mpc}^{-3}\,\mathrm{yr}^{-1}$ (see for example Abadie et al. 2010c), and well below the reach of the present search ($\rho_{\mathrm{GW\text{-}HEN}}^{\mathrm{SGRB}} \lesssim \mathcal{F}_b \times 10^{-2}\,\mathrm{Mpc}^{-3}\,\mathrm{yr}^{-1}$). With $T_{\mathrm{obs}} = 1\,\mathrm{yr}$, an improvement of a factor 10 on the detection distance is required in order to begin constraining the fraction of mergers producing coincident GW−HEN signals.

Guetta et al. (2005) estimate a total rate of long GRBs of $\rho_{\mathrm{LGRB}} \sim 3 \times 10^{-8}\,\mathrm{Mpc}^{-3}\,\mathrm{yr}^{-1}$ after correcting for beaming effects; these sources are closely related to Type II and Type Ibc core-collapse supernovae. The local rate of SNIbc is $\rho_{\mathrm{SNIbc}} \sim 2 \times 10^{-5}\,\mathrm{Mpc}^{-3}\,\mathrm{yr}^{-1}$ (Guetta & Valle 2007), whereas $\rho_{\mathrm{SNII}} \sim 2 \times 10^{-4}\,\mathrm{Mpc}^{-3}\,\mathrm{yr}^{-1}$ (Bazin et al. 2009), relatively close to the obtained limit $\rho_{\mathrm{GW\text{-}HEN}}^{\mathrm{LGRB}} \lesssim \mathcal{F}_b E_{0.01}^{-3/2} \times 10^{-3}\,\mathrm{Mpc}^{-3}\,\mathrm{yr}^{-1}$ under our optimistic assumptions of GW emission in this scenario. A factor 10 only is required in order to begin constraining the fraction of stellar collapse events producing coincident weakly beamed GW-HEN signals, which translates into a required improvement of 2 on the detection dis-

8. CONCLUSIONS

This first joint GW-HEN search using 2007 data, obtained with the ANTARES HEN telescope and the Virgo/LIGO GW interferometers, opens the way to a novel multi-messenger astronomy. Limits on the rate density $\rho_{\mathrm{GW\text{-}HEN}}$ of joint GW-HEN emitting systems were extracted for the first time using the analysis of coincident GW-HEN data. We note that these limits are consistent with the ones obtained in Bartos et al. (2011) derived from independent GW-HEN observations. More stringent limits will be available by performing similar coincidence analyses using other data sets provided by the same instruments.

For instance, the sixth LIGO science run S6 and second and third Virgo science runs VSR2,3 covered the period from 7 July 2009 to 21 October 2010. Meanwhile, the ANTARES telescope has taken data with first 10 then 12 active lines since the end of December 2007. Their enhanced sensitivities should permit a combined analysis to gain the factor required to obtain $\rho_{\mathrm{GW\text{-}HEN}}^{\mathrm{LGRB}} \leq \rho_{\mathrm{SNII/SNIbc}}$ and begin to constrain the fraction of stellar collapse events accompanied by the coincident emission of relativistic jets beamed towards Earth. The analysis of these data is underway, and a similar analysis using data from the LIGO/Virgo S5-VSR1 periods and the IceCube HEN telescope in its 22 string configuration is being finalized.

Future observing runs involving IceCube, KM3NeT (Hernandez-Rey 2009), and the advanced LIGO and advanced Virgo projects (Harry et al. 2010), are likely to coincide as well. They will give other opportunities to look for potential coincident GW-HEN emissions.

9. ACKNOWLEDGMENTS

REFERENCES

Abadie, J., et al. 2010a, ApJ, 715, 1453
—. 2010b, Phys. Rev. D, 82, 102001
—. 2010c, Class. Quantum Grav., 27, 173001
—. 2011, ApJL, 734, L35
—. 2012a, Phys. Rev. D., 85, 122007
—. 2012b, ApJ, 760, 12
—. 2012c, Phys. Rev. D., 85, 082002
Abbasi, R., et al. 2010, ApJ, 710, 346
—. 2011a, Phys. Rev. D., 83, 092003
—. 2011b, Phys. Rev. Lett., 106, 141101
—. 2012a, Nature, 484, 351
—. 2012b, A&A, 539, A60
—. 2012c, ApJ, 744, 1
Abbott, B. P., et al. 2008a, ApJ, 683
—. 2008b, Phys. Rev. Lett., 101, 211102
—. 2008c, Phys. Rev. D., 77
—. 2009a, Phys. Rev. D., 80, 062002
—. 2009b, Rep. Prog. Phys., 72, 076901
—. 2009c, ApJL, 701, L68
—. 2010, ApJ, 715, 1438
Accadia, T., et al. 2012, Journal of Instrumentation, 7, P03012
Acernese, F., et al. 2008, Class. Quantum Grav., 25, 114045
Achterberg, A., et al. 2006, Phys. Rev. Lett., 97, 221101
Adrián-Martínez, S., et al. 2011, in Proceedings of the 32th International Cosmic-Ray Conference, arXiv:1112.0478
Adrián-Martínez, S., et al. 2012a, Astropart. Phys., 36, 204
—. 2012b, ApJ, 760, 53
—. 2012c, Phys. Lett. B, 714, 224
Ageron, M., et al. 2011, Nucl. Instrum. Meth. A, 656, 11
Aglietta, M., et al. 2004, A&A, 421, 399
Aguilar, J. A., et al. 2005, Nucl. Instrum. Meth. A, 555, 132
—. 2007, Nucl. Instrum. Meth. A, 570, 107
—. 2010, Astropart. Phys., 34, 179
—. 2011a, Phys. Lett. B, 696, 16
—. 2011b, Astropart. Phys., 34, 652
Alvarez-Muñiz, J., & Halzen, F. 2001, Phys. Rev. D., 63, 037302
Amram, P., et al. 2003, Astropart. Phys., 19, 253
Anchordoqui, L., & Halzen, F. 2006, Annals of Physics, 321, 2660
Ando, S., & Beacom, J. F. 2005, Phys. Rev. Lett., 95, 061103
Aso, Y., et al. 2008, Class. Quantum Grav., 25, 114039
Athar, H., Kim, C. S., & Lee, J. 2006, Mod. Phys. Lett. A, 21, 1049
Baret, B., et al. 2011, Astropart. Phys., 35, 1
Barthelmy, S. D., et al. 2005, Space Sci. Rev., 120, 143
Bartos, I., et al. 2011, Phys. Rev. Lett., 107, 251101
Bazin, G., et al. 2009, A&A, 499, 653
Berezinsky, V., Sabancilar, E., & Vilenkin, A. 2011, Phys. Rev. D., 84, 085006
Bhat, P. N., et al. 2004, in AIP Conf. Ser., Vol. 727, Gamma-Ray Bursts: 30 Years of Discovery, ed. E. Fenimore & M. Galassi, 684
Bhattacharjee, P. 1989, Phys. Rev. D., 40, 3968
Braccini, S., et al. 2005, Astropart. Phys., 23, 557
Brady, P. R., Wiseman, A. G., & Creighton, J. D. E. 2004, Class. Quantum Grav., 21, S1775
Bromberg, O., Nakar, E., & Piran, T. 2011, ApJL, 739, L55
Burrows, A., et al. 2007, ApJ, 664, 416
Chapman, R., et al. 2007, MNRAS, 382, L21

Chatterji, S., et al. 2006, Phys. Rev. D., 74, 082005
Chen, H.-Y., & Holz, D. E. 2012, arXiv:1206.0703
Corsi, A., & Mészáros, P. 2009, ApJ, 702, 1171
Corsi, A., & Owen, B. J. 2011, Phys. Rev. D., 83, 104014
Coward, D. M. 2005, MNRAS, 360, L77
Creighton, J. D. E., & Anderson, W. G. 2011, Gravitational-Wave Physics and Astronomy: An Introduction to Theory, Experiment and Data Analysis (Wiley-VCH, Hoboken, NJ, USA)
Damour, T., & Vilenkin, A. 2000, Phys. Rev. Lett., 85, 3761
Damour, T., & Vilenkin, A. 2001, Phys. Rev. D., 64, 064008
Davies, M. B., et al. 2002, ApJL, 579, L63
de Freitas Pacheco, J. A. 1998, A&A, 336, 397
Dietz, A., Fotopoulos, N., Singer, L., & Cutler, C. 2012, arXiv:1210.3095
Dimmelmeier, H., et al. 2008, Phys. Rev. D., 78, 065056
Faber, J. A., & Rasio, F. A. 2012, Living Rev. Relat., 15, 8
Fryer, C., Holz, D., & Hughes, S. 2002, ApJ, 565, 430
Fryer, C., & New, K. 2011, Living Rev. Relat., 14
Gehrels, N., Ramirez-Ruiz, E., & Fox, D. B. 2009, ARA&A, 47, 567
Gehrels, N., et al. 2004, ApJ, 611, 1005
Gill, R., & Heyl, J. S. 2010, MNRAS, 407, 1926
Gorham, P. W., et al. 2010, Phys. Rev. D., 82, 022004
Guetta, D., & Piran, T. 2006, A&A, 453, 823
Guetta, D., Piran, T., & Waxman, E. 2005, ApJ, 619, 412
Guetta, D., & Stella, L. 2009, A&A, 498, 329
Guetta, D., & Valle, M. D. 2007, Astropart. Phys., 657, L73
Guetta, D., et al. 2004, Astropart. Phys., 20, 429
Halladjian, G. 2010, PhD thesis, Université de la Méditérranée–Aix Marseille II, Marseilles, France
Halzen, F., Landsman, H., & Montaruli, T. 2005, TeV photons and Neutrinos from giant soft-gamma repeaters flares
Harry, G. M., et al. 2010, Class. Quantum Grav., 27, 084006
He, H.-N., et al. 2012, ApJ, 752, 29
Hernandez-Rey, J. J. 2009, J. Phys. Conf. Ser., 171, 012047
Hill, C. T., Schramm, D. N., & Walker, T. P. 1987, Phys. Rev. D., 36, 1007
Hjorth, J., & Bloom, J. S. 2011, in Gamma-Ray Bursts, ed. C. Kouveliotou et al. (Cambridge, UK: Cambridge University Press), 169–190
Horiuchi, S., & Ando, S. 2008, Phys. Rev. D., 77, 063007
Hümmer, S., Baerwald, P., & Winter, W. 2012, Phys. Rev. Lett., 108, 231101
Hurley, K. 2011, Adv. Space Res., 47, 1326
Ioka, K. 2001, MNRAS, 327, 639
Ioka, K., et al. 2005, ApJ, 633, 1013
Kelley, L. Z., Mandel, I., & Ramirez-Ruiz, E. 2012, arXiv:1209.3027
Khokhlov, A. M., et al. 1999, ApJL, 524, L107
Kibble, T. W. B. 1976, J. Phys. A Math. Gen., 9, 1387
Kiuchi, K., et al. 2011, Phys. Rev. Lett., 106, 251102
Kobayashi, S., & Mészáros, P. 2003, ApJ, 589, 861
Kobayashi, S., & Meszaros, P. 2003, ApJ, 585, L89
Kotake, K. 2011, Multiple physical elements to determine the gravitational-wave signatures of core-collapse supernovae, arXiv:1110.5107
Lazzati, D., et al. 2012, ApJ, 750, 68

Le, T., & Dermer, C. D. 2007, Astrophys. J., 661, 394
Levin, Y., & van Hoven, M. 2011, MNRAS, 418, 659
Li, Z. 2012, Phys. Rev. D., 85, 027301
Liang, E., et al. 2007, ApJ, 662, 1111
Lunardini, C., & Sabancilar, E. 2012, Phys. Rev. D., 86, 085008
Lyutikov, M. 2006, MNRAS, 367, 1594
MacFadyen, A. I., & Woosley, S. E. 1999, ApJ, 524, 262
Mattila, S., et al. 2012, ApJ, 756, 111
Meegan, C., et al. 2009, ApJ, 702, 791
Mereghetti, S. 2011, Adv. Space Res., 47, 1317
Mészáros, P. 2006, Rep. Prog. Phys., 69, 2259
Meszaros, P., & Waxman, E. 2001, Phys. Rev. Lett., 87, 171102
Metzger, B. D., et al. 2011, MNRAS, 413, 2031
Modjaz, M. 2011, Astron. Nachr., 332, 434
Mosquera Cuesta, H. J., & González, D. M. 2001, Phys. Rev. B., 500, 215
Murase, K., & Nagataki, S. 2006, Phys. Rev. Lett., 97, 051101
Murase, K., et al. 2006, ApJL, 651, L5
Nakar, E. 2007, Phys. Rept., 442, 166
Nakar, E., Gal-Yam, A., & Fox, D. B. 2006, ApJ, 650, 281
Nissanke, S., Kasliwal, M., & Georgieva, A. 2012, arXiv:1210.6362
O'Connor, E., & Ott, C. D. 2011, ApJ, 730, 70
Ott, C. D. 2009, Class. Quantum Grav., 26, 063001
Ott, C. D., et al. 2011, Phys. Rev. Lett., 106
Ott, C. D., et al. 2012, Phys. Rev. D., 86, 024026
Papaloizou, J. C., & Savonije, G. J. 1991, MNRAS, 248, 353
Papaloizou, J. C. B., & Pringle, J. E. 1984, MNRAS, 208, 721
Piran, T. 2005, Rev. Mod. Phys., 76, 1143
Piro, A. L., & Pfahl, E. 2007, ApJ, 658, 1173
Polchinski, J. 2004, Introduction to Cosmic F- and D-Strings, Lecture notes – Cargèse summer school, arXiv:hep-th/0412244
Popham, R., Woosley, S. E., & Fryer, C. 1999, ApJ, 518, 356
Pradier, T. 2009, Nucl. Instrum. Meth. A, 602, 268

Razzaque, S., Mészáros, P., & Waxman, E. 2003, Phys. Rev. D., 68, 083001
—. 2005a, Phys. Rev. Lett., 94, 109903
—. 2005b, Mod. Phys. Lett. A, 20, 2351
Scheidegger, S., et al. 2010, A&A, 514, A51
Scholten, O., et al. 2009, Nucl. Instrum. Meth. A, 604, 102
Shibata, M., & Taniguchi, K. 2011, Living Rev. Relat., 14, 6
Siemens, X., et al. 2006, Phys. Rev. D., 73, 105001
Soderberg, A. M., et al. 2006, Nature, 442, 1014
Soderberg, A. M., et al. 2010, Nature, 463, 513
Sutton, P. J., et al. 2010, New J. Phys, 12, 053034
Takiwaki, T., & Kotake, K. 2011, ApJ, 743
Thompson, C., & Duncan, R. C. 1995, MNRAS, 275, 255
Thorne, K. S. 1987, in 300 Years of Gravitation, ed. S. W. Hawking & W. Israel (Cambridge, UK: Cambridge University Press)
van Putten, M. H., et al. 2004, Phys. Rev. D., 69, 044007
Virgili, F. J., Liang, E.-W., & Zhang, B. 2009, MNRAS, 392, 91
Wang, X.-Y., et al. 2007, Phys. Rev. D., 76, 083009
Was, M. 2011, PhD thesis, Universit Paris Sud, LAL 11-119
Was, M., et al. 2012, Phys. Rev. D., 86
Waxman, E., & Bahcall, J. 1997, Phys. Rev. Lett., 78, 2292
Waxman, E., & Loeb, A. 2001, Phys. Rev. Lett., 87, 071101
White, D. J., Daw, E. J., & Dhillon, V. S. 2011, Class. Quantum Grav., 28, 085016
Winter, W. 2012, Advances in High-Energy Physics, 2012, 586413
Woosley, S. E. 1993, ApJ, 405, 273
Woosley, S. E., & Heger, A. 2006, ApJ, 637, 914
Zhang, B.-B., et al. 2012, ApJ, 756, 190
Zink, B., Kokkotas, K. D., & Lasky, P. D. 2012, Phys. Rev. D., 85, 024030